EFFECTS OF SOLID SOLUTION ON THE HIGH-LOW INVERSION OF CRISTOBALITE AND THE STABILIZATION OF HIGH CRISTOBALITE

by

Tawei Sun

Dissertation submitted to the Faculty of the

Virginia Polytechnic Institute and State University

in partial fulfillment of the requirements for the degree of

DOCTOR OF PHILOSOPHY

in

Materials Engineering Science

APPROVED:

J. J. Brown, Jr.

G. V. Gibbs

R. E. Swanson

J. L. Lytton

F. D. Bloss

December, 1989

Blacksburg, Virginia

Effects of Solid Solution on the High-Low Inversion of Cristobalite and the Stabilization of High Cristobalite

by

Tawei Sun

Committee Chairman: Jesse J. Brown

(ABSTRACT)

The inversion temperature of cristobalite was investigated by incorporating TiO_2, $AlPO_4$, and BPO_4 into the cristobalite phase using solid state reactions. The combination of TiO_2 and $AlPO_4$ proved to be most effective in lowering the inversion temperature of cristobalite. Phase diagrams at the high silica corner were constructed for the respective systems. High cristobalite was stabilized for compositions prepared from the $CaO-Al_2O_3-SiO_2$ and $CuO-Al_2O_3-SiO_2$ system using sol-gel processing. The stabilization mechanism is attributed to the surface energy effect resulting from the formation of fine crystals. The structural evolution from the x-ray amorphous gel to high cristobalite was examined by FTIR and Raman spectroscopy. The thermal expansion of the stabilized high cristobalite was characterized by high temperature x-ray. Changes in bond angle continue to dominate the thermal expansion of high cristobalite.

Acknowledgements

The author wishes to thank Dr. Jesse J Brown for his enormous support throughout the years. The author would also like to thank Dr. G. V. Gibbs, Dr. F. D. Bloss, Dr. R. E. Swanson, and Dr. J. L. Lytton for serving on the committee.

Thanks are also extended to , , , and , who have been of tremendous help. Especially, I want to thank my parents and my sisters as usual and as always.

Table of Contents

List of Tables

List of Figures

I. Introduction

Polymorphic transformation due to changes in external conditions, especially temperature, has been a major barrier to the application of some high temperature ceramics. Failure often occurs as a result of abrupt dimensional changes upon phase transformation. The relatively open structure with strong primary bonds makes ceramics highly susceptible to polymorphic transformation. In order to avoid the breaking of bonds, a low activation energy path is usually chosen by rearranging atoms in the secondary coordination. Phase transformation of this kind can be considered as thermodynamics-controlled, as opposed to kinetics-controlled, because of the instantaneous completion of the process. Another important cause, perhaps the most frequently encountered, for the failure of ceramics is the thermal shock generated by thermal expansion. Although ceramics in general have much lower thermal expansion when compared to that of metals and polymers, the lack of plasticity greatly reduces the acceptable thermal expansion range for ceramics to be useful at high temperatures. Therefore, phase transformation has to be eliminated and thermal expansion reduced before use can be made of high temperature structural ceramics. The thermal expansion data, however, need to be examined with caution. A nominally low thermal expansion can sometimes result from the highly anisotropic expansion in different crystallographic directions, for example, contraction in one axis and expansion in the other. In this case, the resultant low expansion may be misleading. Depending on the degree of anisotropy, it can actually weaken the

material through formation of microcracks.

High cristobalite or β-cristobalite has been of particular interest to those who seek materials with high thermal shock resistance and low cost. The nearly zero thermal expansion of high cristobalite between 300 and 1000°C has been frequently noted. Its isotropic expansion makes it even more appealing. However, the spontaneous transformation from high cristobalite to low cristobalite, which creates large discontinuous volume change, makes its potential applications limited. Because of the nature of the high-low transformation, tremendous difficulty was encountered in the past in attempting to stabilize high cristobalite. The difficulty primarily arises from the apparent lack of a kinetic barrier in the high-low transformation as evidenced by the speed of transformation.

The goal of this study is to stabilize high cristobalite using thermodynamic considerations and both solid state and sol-gel processing. Alternatively, the goal can be approached by extending the stability region of high cristobalite, provided that the transformation temperature shows a continuous decrease with the formation of solid solution.

A. Polymorphism of Silica

Depending on the temperature and pressure, more than 17 silica polymorphs are known to exist for this chemically simple species.[1] Nonetheless, its crystal chemical behaviors appear to be one of the most complex and difficult to understand. Two types of polymorphic

transformation are involved in the silica system, displacive and reconstructive, as proposed by Buerger.[2] Both are based on the crystallographic changes and kinetic characteristics that occur upon transformation.

A highly symmetrical structure (Fig. 1) can transform to a completely different assemblage by reconstructive transformation, or to a slightly distorted form by displacive transformation.[3] Reconstructive transformation involves temporary breaking of bonds in the first coordination, while only rearrangement of secondary coordination takes place in displacive transformation. The displacive transformation of silica is also referred to as the high-low inversion, the low temperature form being the derivative of the high temperature. The SiO_4 tetrahedral units remain intact, but the relative orientation is changed drastically. The kinetics are entirely different between the displacive and reconstructive transformation. In the displacive transformation, neither bonds between atoms are broken, nor is an energy barrier encountered, and therefore thermally activated diffusion in not required. Consequently a displacive transformation proceeds with a very high speed equivalent to that of heat transmission. On the other hand, a reconstructive transformation requires large thermal energy for the nucleation and growth process necessary to form a completely different phase. A reconstructive transformation proceeds sluggishly because of the kinetic barrier. Since the thermal energy is usually unavailable at low temperatures, high temperature polymorphs commonly exist indefinitely below their stability region.

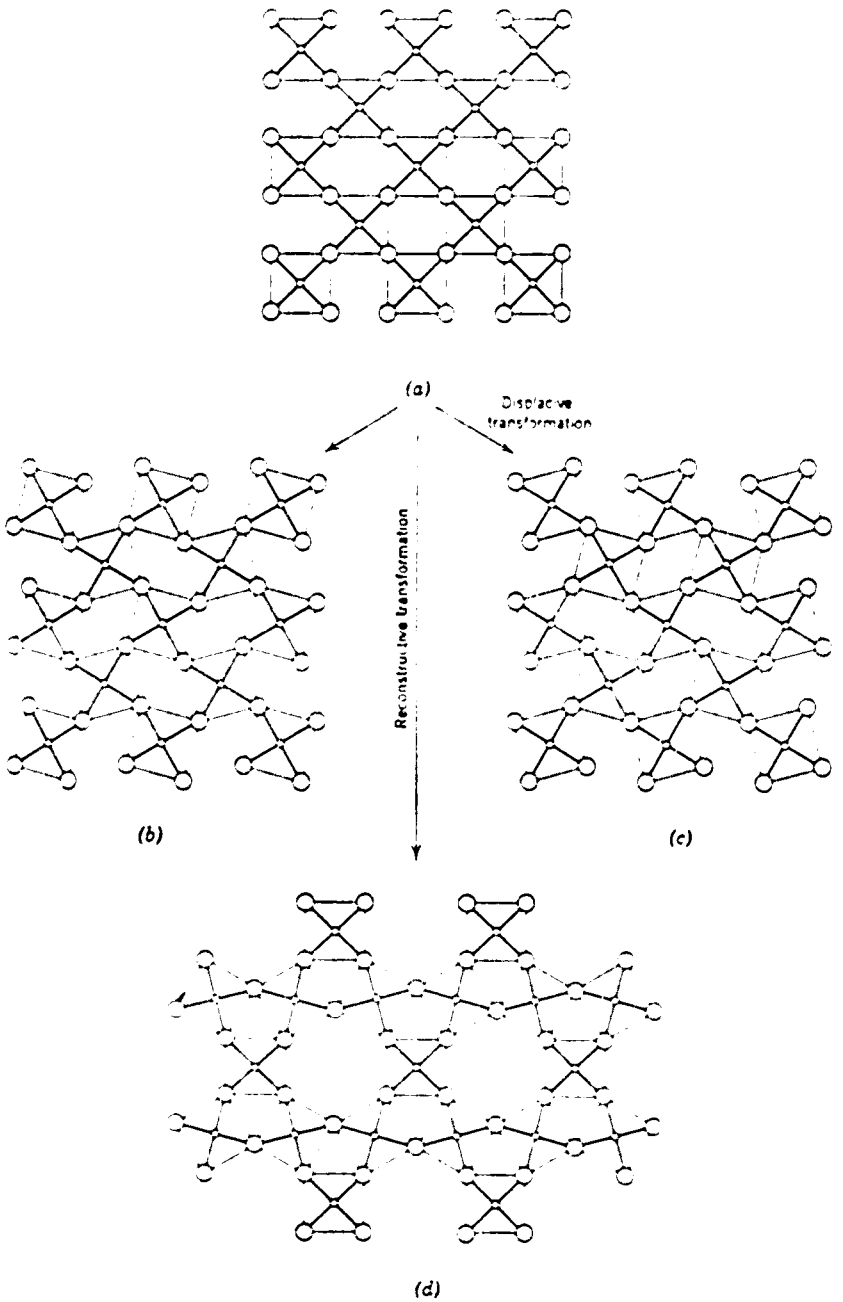

Figure 1. A highly open structure (a) showing displacive transformation into a collapsed form (b) and (c) or reconstructive transformation into a completely different form (d) (ref. 3).

The transformations involving the permutations among quartz, tridymite, and cristobalite are characterized by the reconstructive type. Meanwhile, high-low transformations occur reversibly within each phase. The stability region of the silica polymorphs is shown in Fig. 2.[4] The pressure shown in the diagram is assumed to be near one atmosphere and the high pressure forms are ignored. The equilibrium temperatures between quartz and tridymite and also between tridymite and cristobalite were determined by indirect experimental results, since heat treatment of pure SiO_2 under dry conditions can not yield tridymite.[5] The equilibrium temperatures were determined either by hydrothermal methods or by the addition of a mineralizer. Therefore, it becomes questionable if it still represents a true one-component system under those conditions.

Normal practice in interpreting phase diagrams cannot be directly applied to the silica polymorphs, since a metastable phase often obscures the thermodynamically stable phase. The polymorphic transformations in the silica system seem to follow what was suggested by Ostwald[6]: "In all reactions the most stable state is not straightaway reached, but the next less stable, or that state which is the least stable of the possible states." Unless the thermal history of the sample and the processing method are given, one has to follow the metastable boundaries shown in Fig. 2 in order to predict the phase changes. Therefore, when β-cristobalite is cooled below 1470°C, it does not transform to tridymite between 867 to 1470°C, nor does it transform to quartz below 867°C. Instead, displacive transformations take place between 200 to 270°C, where β-cristobalite converts to

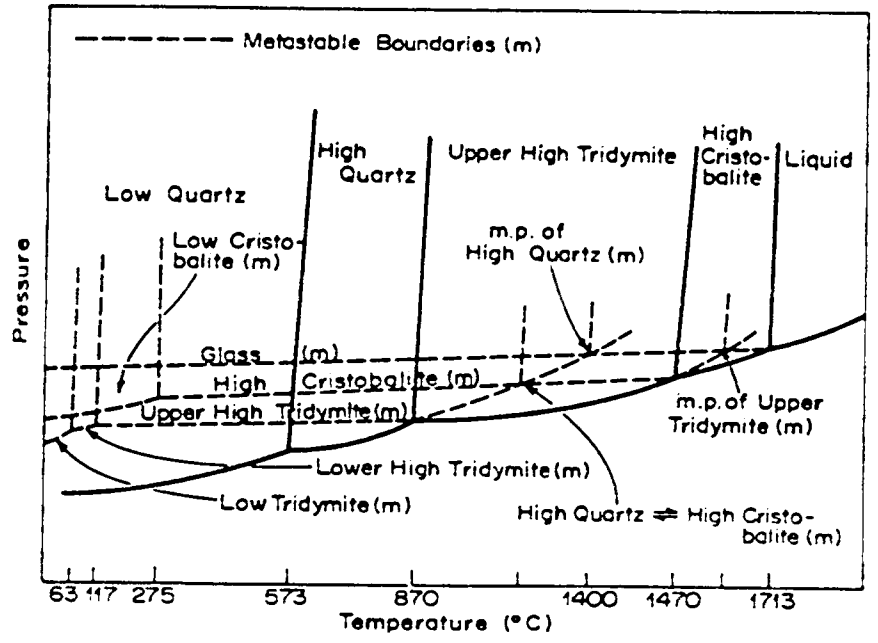

(a)

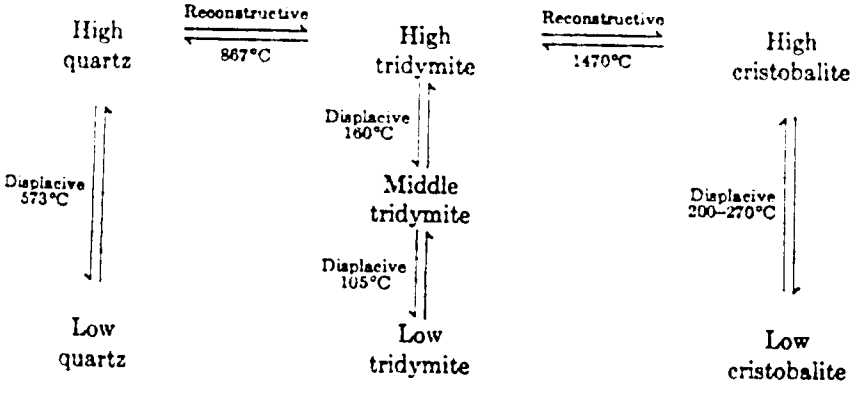

(b)

Figure 2. The stability region of silica (a) and its polymorphic transformation (b) (ref. 4).

α-cristobalite. Upon heating, α-quartz transforms to β-quartz at 573°C via a displacive transformation, which is both thermodynamically and kinetically favored. Above 867°C, β-quartz can either transform to β-cristobalite or melt at temperatures below 1700°C, depending on the heating rate, but not to tridymite.[7] The transformation from quartz to cristobalite involves a phase-boundary-controlled conversion from quartz to a transitional amorphous phase followed by a first order conversion of the amorphous phase to cristobalite.[8]

Tridymite has never been synthesized in the pure state under atmospheric pressure; therefore, it is often argued that tridymite is not a true polymorph of silica. The presence of mineralizers such as tungstates or alkali flux is required for the formation of tridymite at ambient pressure. Pure tridymite can only be prepared in the presence of H_2O.[9] Under these conditions, quartz converts to tridymite between 867 and 1470°C, presumably by dissolving the metastable quartz and permitting tridymite to crystallize. Above 1470°C, tridymite can transform to cristobalite without the presence of a mineralizer. Once formed, tridymite undergoes a series of displacive transformations from high to middle and then to low tridymite upon cooling.

The amorphous phase observed in the quartz-to-cristobalite conversion and the necessary conditions in forming tridymite suggest that a complex dissolution and crystallization precess is involved in the reconstructive transformation. The nucleation process may require too much thermal energy, and meanwhile enough energy is localized to cause incipient melting and subsequent crystallization. It was found

that crystallization almost always started on the surface, indicating heterogeneous nucleation, and that particle size played an important role in the transformation rate.[10]

B. High-Low Inversion of Cristobalite

The principal characteristics associated with the high-low inversion of cristobalite are[1]:

1. The inversion completes in seconds when the inversion temperature is reached, both on heating and cooling.
2. The inversion process is reversible with respect to temperature.
3. Temperature hysteresis is usually observed with the inversion occurring at higher temperature on heating than cooling.
4. Unlike the phases related by reconstructive transformations, the energy difference between the high and low polymorph is small but finite.
5. The presence of a second phase in the form of a mechanical mixture does not catalyze the inversion process, nor does it affect the inversion temperature.

The high-low inversion of cristobalite differs from that of quartz in that, compared to 573°C for quartz, the inversion temperatures of cristobalite may lie between 200 and 272°C. The inversion temperatures are strongly dependent on the thermal history of cristobalite, particularly on the temperature at which cristobalite is formed.[11,12] Higher formation temperatures usually result in higher inversion temperatures. The difference in inversion temperatures resultant from

differing formation temperatures can be as large as 48°C on heating, and 27°C on cooling.[13] Large hysteresis and narrow inversion range are usually associated with the high inversion temperature.

Cristobalite not only has a wide inversion range for samples from different origins, but also shows a statistical distribution in the inversion temperatures within a specific sample. It was found under the polarizing microscope that different crystallites crushed from the same aggregate transformed at different temperatures on both heating and cooling.[14] The transformation time was observed to be less than 0.1 second. The results indicate that each crystallite has it own characteristic inversion temperature. Therefore, the inversion temperature reported for cristobalite actually represents the mean inversion temperature of the specific specimen. Moreover, the transformation temperature was even found to vary in a single crystal. In a high temperature x-ray study of cristobalite, Peacor detected a variation in the inversion temperature of nearly 10°C in a single crystal.[15] The (102) reflection which is extinct in high cristobalite was used to diagnose the inversion process. On heating, the intensity of the (102) peak decreased continuously between 223° and 230°C and became unobservable at 230°C. On cooling, the (102) peak became observable at 215°C and showed a continuous increase in intensity until a final steady-state condition was reached at 204°C. The distribution in the inversion temperatures also explains why the thermal expansion of cristobalite is not exactly discontinuous during inversion. Therefore, the slightly rounded expansion curve does not imply second order transformation, and the high-low inversion of

cristobalite should be characterized by a first order transformation.[16]

The variable inversion temperature of cristobalite is often related to the degree of crystallinity. It was found that well-crystallized cristobalite, which was formed at high temperature, transformed at the highest temperature, and various degrees of disorder in the high cristobalite structure were proposed.[17] The state of disorder depends on the formation temperature of high cristobalite. Poorly-crystallized cristobalite corresponds to a high degree of disorder, and therefore high configurational entropy. At equilibrium, the inversion temperature varies inversely with the entropy change, assuming the enthalpy change is constant. Because of the high degree of disorder, cristobalite formed at low temperature usually exhibits a low inversion temperature. It was suggested that crystal size can also affect the inversion temperature.[2]

High cristobalite rarely exists at ambient temperature because of the nature of the high-low inversion. Nonetheless, some examples show that high cristobalite can be retained under special conditions. The first one is when high cristobalite was embedded in a glass matrix.[18] The inversion was suppressed by the mechanical constraint generated from the glass matrix. However, the inversion proceeded when the constraint was removed. Another example was found in opal.[2,19] Extensive x-ray studies of various opals showed that the diffraction patterns consisted of high cristobalite with different degrees of crystallinity.

C. Structure of Cristobalite Polymorph

The crystal structure of low cristobalite belongs to the tetragonal system with the space group $P4_12_1$ (or $P4_32_1$).[20,21] Each unit cell contains 4 SiO_2 molecules with cell dimensions a = 4.97 A, and c = 6.94 A. According to Dollase[20], the atomic positions are:

Si (a): u, u, 0; -u, -u, 1/2; 1/2 - u, u + 1/2, 1/4;
u + 1/2, 1/2 - u, 3/4,

O (b): x, y, z; -x, -y, z + 1/2; 1/2 - y, x + 1/2, z + 1/4;
y + 1/2, 1/2 - x, z + 3/4; y, x, -z; -y, -x, 1/2 - z;
1/2 - x, y + 1/2, 1/4 - z; x + 1/2, 1/2 - y, 3/4 - z,

where u = 0.3000, x = 0.2398, y = 0.1032, and z = 0.1784. The interatomic distances and angles of the silicon tetrahedra are summarized in Table 1. The data indicate that the framework structure is made up of irregular SiO_4 tetrahedra. Fig. 3 shows the projection of low cristobalite on different planes.[22] The numbers in each projection represent the height fraction of the axis perpendicular to the drawing.

Compared to low cristobalite, the structure of high cristobalite is not as well established because of the uncertainties in the oxygen positions. The high cristobalite structure was first investigated by Wyckoff[23] using devitrified silica glass. The space group was identified as Fd3m with cubic cell edge a = 7.13 A. Each unit cell contains 8 SiO_2 molecules with Si atoms assuming diamond lattice positions and oxygen atoms at midway between two Si atoms. The Si-O distance and the Si-O-Si bond angle were determined to be 1.54 A and

Table 1. Interatomic Distances and Angles of Low Cristobalite (from ref. 21)

	23°C	200°C
Si-O (A)	1.599	1.605
	1.606	1.590
O-Si-O (°)	108.2	108.27
	109.17	108.64
	109.99	109.69
	111.27	112.22
Si-O-Si (°)	146.70	148.

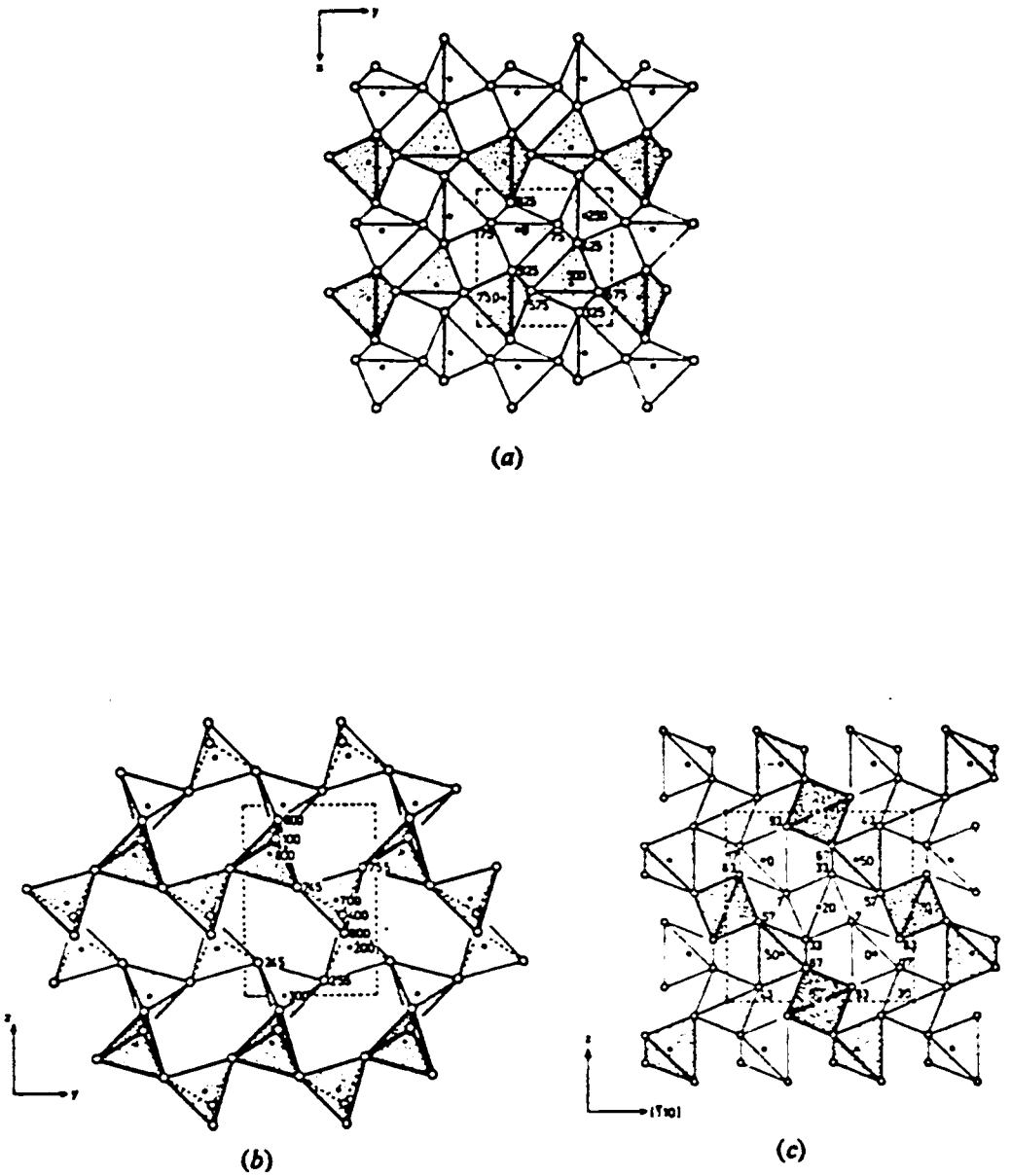

Figure 3. The projection of low cristobalite on (a) (001), (b) (100), and (c) (110) plane of the $P4_12_12$ unit cell (ref. 22).

180^{o}, respectively. The structure can be viewed as consisting of SiO_4 tetrahedral sheets stacked in an ABC sequence along the [111] direction. Fig. 4 shows the orthographic projection of the ideal high cristobalite structure on the (001) plane. A different structure was proposed by Barth[24], whose data showed a $P2_13$ space group with the Si-O distance between 1.58 and 1.68 A and the Si-O-Si bond angle less than 180^{o}. Nieuwenkamp[25] arrived at a conclusion similar to that of Wyckoff (Fd3m), except that the oxygen atoms are randomly distributed on a circle of radius of 0.3 to 0.55 A normal to the Si-Si axis.

The structure proposed by Barth is generally ruled out because of the uncertainty in sample purity. However, the structures determined by Wyckoff and Nieuwenkamp are also questionable. The Si-O distance and Si-O-Si angle from Wyckoff's data differ considerably from the values observed for silica and silicates. The thermal amplitude of the oxygen atoms in Nieuwenkamp's results appears to be too large at temperatures far below the melting temperature of cristobalite. Therefore, the structure of high cristobalite was reinvestigated by Peacor[15] and Leadbetter et al.[26,27] Both results are similar and confirm the space group to be Fd3m with the Si-O distance equal to 1.61 A and the Si-O-Si angle varying continuously with temperatures.

Although the space group remains the same, the interpretation of the oxygen position is different from those previously proposed. Fig. 5 shows the local atomic arrangement in high cristobalite. The Si atoms are placed in the special positions (a) of the space group Fd3m, and the 16 oxygen atoms are distributed among the 96 (h) positions. Each oxygen atom can locate at one of the six distinct but

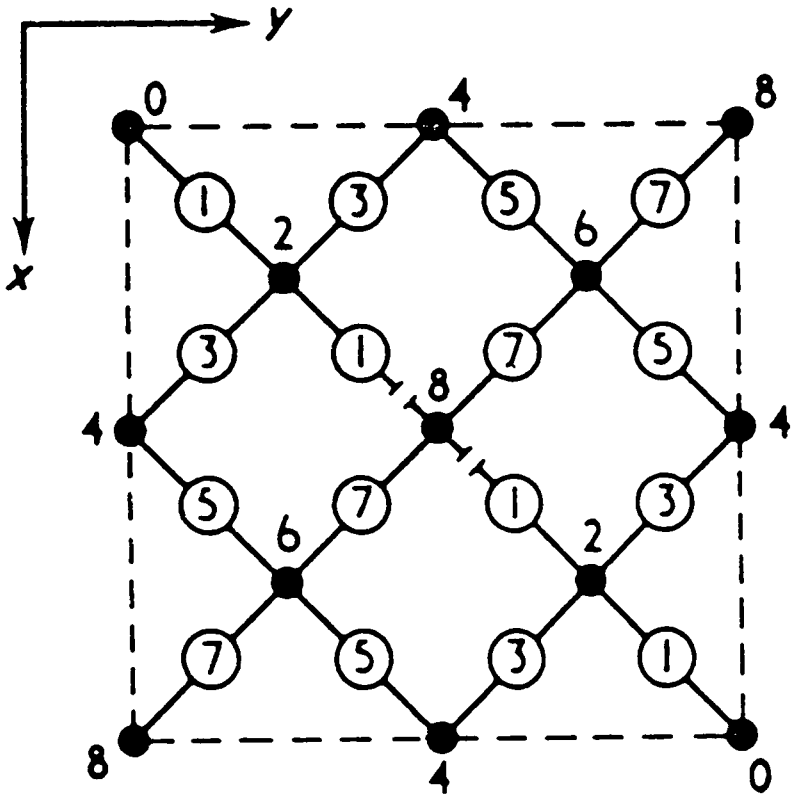

Figure 4. The projection of the idealized high cristobalite structure on (oo1) plane. Heights are marked in units of c/8 (ref. 36).

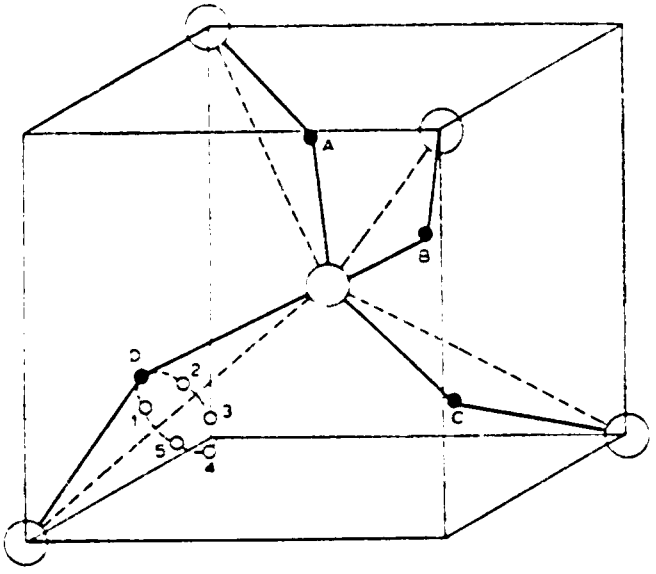

(a)

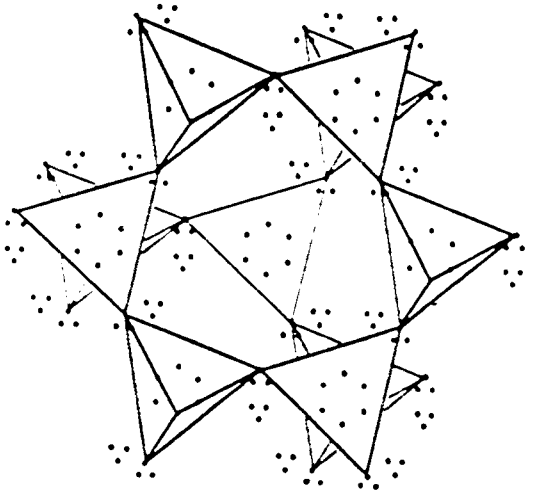

(b)

Figure 5. The local atomic arrangement of high cristobalite (a) and its projection on (111) plane (b). The small cricle in (a) shows the six possible oxygen positions (ref. 27).

equivalent positions. Therefore, the only possible interpretation of the oxygen distribution is to assume the existence of short range order in domains of lower symmetry. In each domain, a subset of one sixth of the 96 (h) positions is occupied, and the domains of each of the six possible subsets occur with equal probability. The domain structure determined by Leadbetter et al[26] was based on the symmetry of F4d2 as shown in Fig. 6. The domain cannot extend more than a few unit cells since large strains will be generated at the domain boundaries as evidenced by the large temperature factor found in the structure analysis.[27] It also implies that micro-twinning may exist in the domain structure. Therefore, the determined high cristobalite structure is considered the average structure of all the domains. In order to yield the symmetry of Fd3m, considerable disorder has to exist in the structure. This may explain the fact that the inversion temperature of cristobalite is not fixed, and that each crystallite has its own characteristic inversion temperature. Upon inversion, the Si atoms in the α phase simply move to the special positions (a) in the β phase, whereas there are on the average six equivalent positions of higher symmetry in the β phase for each oxygen atom in the α phase.

According to O'Keefe and Hyde[22], the structures of low cristobalite and high cristobalite are topologically related to the ideal high cristobalite or the C9 structure originally proposed by Wyckoff. Low cristobalite can be derived from the C9 structure by rotating the SiO_4 tetrahedra along the [0-10], [001], and [010] axis in sequence. Likewise, high cristobalite can be obtained by rotation along the [00-1],[001], and then the [00-1] axis in the C9 structure.

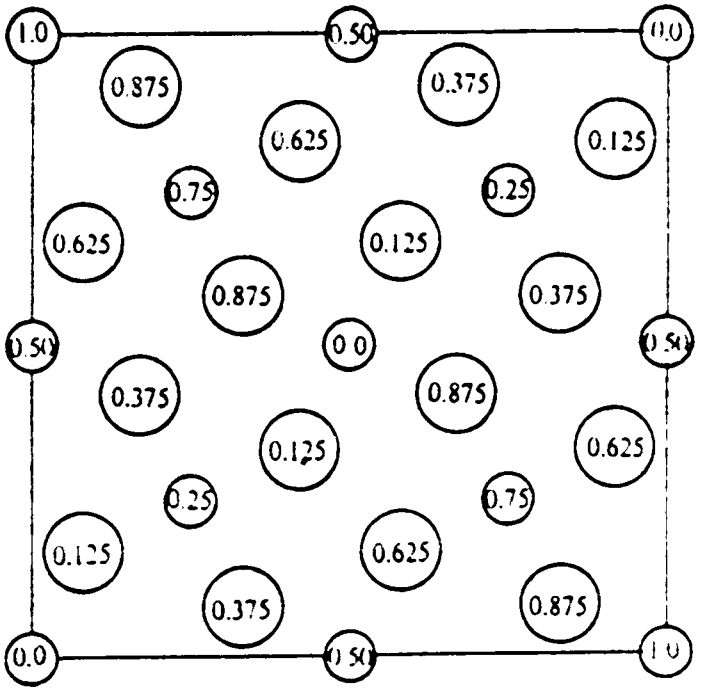

Figure 6. The projection along the c-axis of the domain structure of high cristobalite (ref. 26).

It appears that the α and β phases can be transformed to each other via the C9 structure. However, this requires the Si-O-Si angle to be 180° at an intermediate stage during the transformation. A more direct mechanism may be operative as shown in Fig. 7. The β phase can be transformed to the α phase if the tetrahedra centered at a quarter height are rotated clockwise along their edges marked with heavy arrows. At the same time, the central horizontal row of tetrahedra rotates along axes normal to the plane of projection and translates slightly.

D. Thermal Expansion of Cristobalite

Thermal expansion, which occurs as a result of anharmonic atomic vibrations, is closely related to the structural characteristics.[28,29] Structures of ceramics can be regarded to consist of various cation polyhedra. The size and geometry of the polyhedra, as well as the ways the polyhedra are linked together, are predicted by Pauling's rules.[30] The thermal expansion behavior of those polyhedra directly manifests itself on the expansion of the bulk. Some general rules can be made for the thermal expansion of the cation polyhedra.[31]

1. The thermal expansion of a given type of polyhedron appears to be the same, although the structure to which it belongs may be different.
2. For the same structure, the thermal expansion of a given type of polyhedron is almost the same, regardless of the cation species.
3. The thermal expansion of the polyhedra increases with the

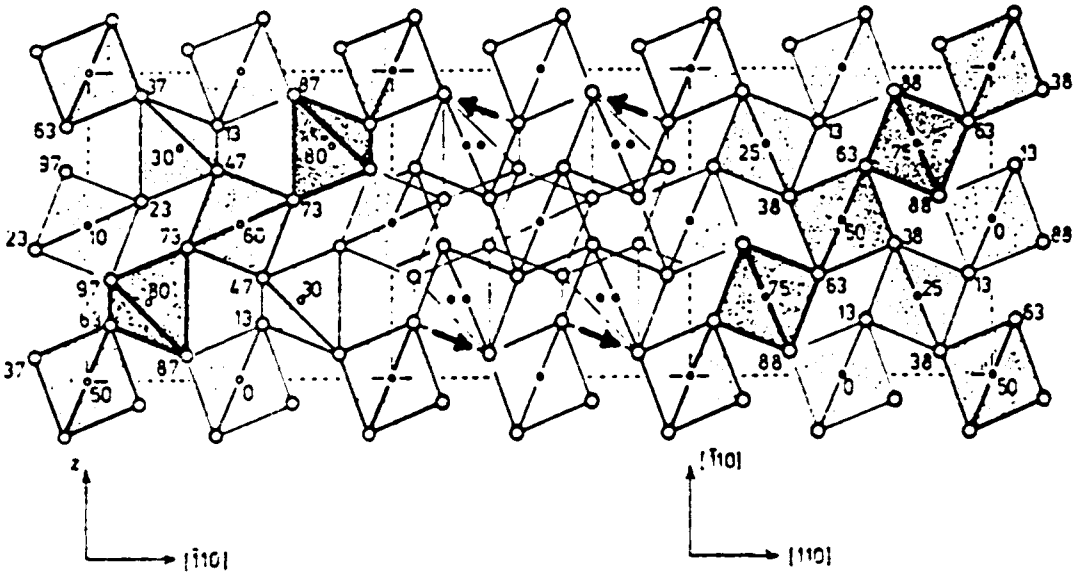

Figure 7. The high-low inversion from high cristobalite (on the right) to low cristobalite (on the left) (ref. 22).

coordination number of the cation.

4. Polyhedral distortion has not been found to affect the thermal expansion significantly.

Therefore, it seems possible to assign a characteristic thermal expansion value to each polyhedron. For simple structures composed of only one type of polyhedron, the thermal expansion of the bulk is sometimes identical to that of the polyhedron. For a number of structures, a simple correlation was found between the thermal expansion β and the bond strength S, where S is defined as the valence of the cation divided by its coordination number[32]. Fig. 8 shows that the thermal expansion is inversely proportional to the square of the bond strength. The results also indicate that strong interatomic forces (short bond length) are associated with low thermal expansion and that covalent crystals have lower expansion than ionic crystals.

In many cases, however, the thermal expansion behaviors are dominated by the configuration of the polyhedra instead of the polyhedra expansion. Typical examples are silica polymorphs and most of the framework silicates where SiO_4 tetrahedra show nearly zero expansion while large expansion was observed. The highly rigid SiO_4 tetrahedra do not imply low expansion in the framework structure. The small force constant of the bridging oxygen ions makes the corner-linked tetrahedra specially susceptible to bending or tilting. In other words, it is the change in bond angle that causes the structure to expand. Thermal expansion of this kind was found to parallel the changes of the bond angle.[33-36] In addition, the thermal expansion resulting from the tilting effect is generally much larger when

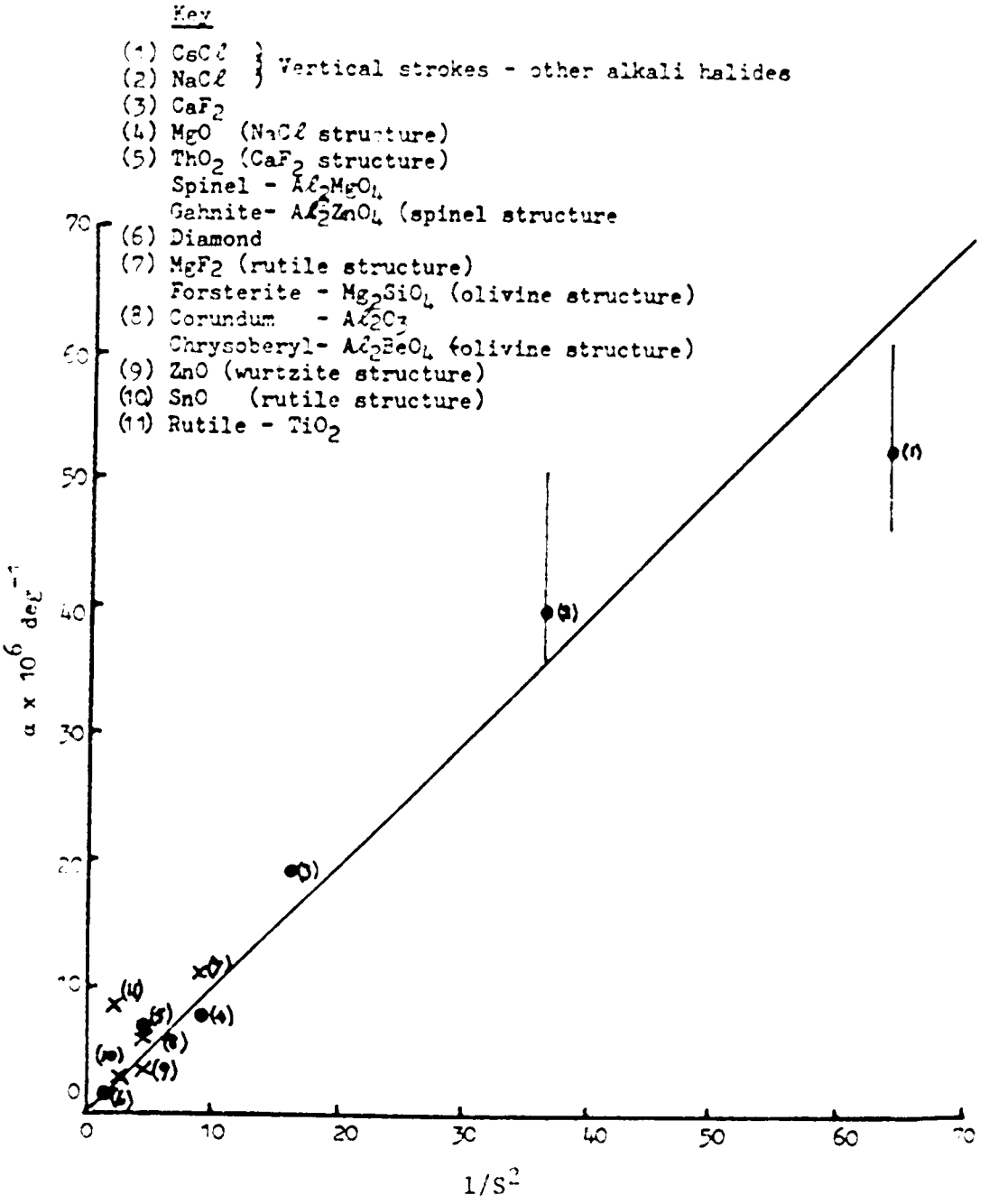

Figure 8. Thermal expansion coefficient versus $1/S^2$ for structures that cannot tilt (ref. 32).

compared to the expansion caused by the increase in bond length.[37] The tilting effect can be greatly reduced if the bridging oxygen ions in the framework are partially or completely replaced by N to form Si_2ON_2 or Si_3N_4.[38] Tilting of the Si tetrahedra in this case will create considerable distortion due to the higher coordination number of N.

According to Taylor[39], the thermal expansion of framework structures can be characterized by three stages, from partially collapsed to the fully extended states as shown in Fig. 9. The change in bond angle often culminates in a phase transformation in the framwork structures. Therefore, the first stage takes place between room temperature and the transformation temperature. The transformation is usually of the displacive type. Expansion corresponding to this stage is the largest and the bond angle shows the greatest increase. The second stage starts at the transformation temperature and ends at a temperature where the bond angle ceases to change and the structure has reached the fully extended state. moderate expansion is observed in this stage, even though the structure has transformed to the high temperature form. In the final stage, the structure shows almost zero expansion or even contraction. The slightly negative expansion is attributed to the increase in the anisotropic thermal vibration of the oxygen atoms, which results in an apparent shortening of the bond length.[40]

The changes of the cristobalite structure from the partially collapsed to fully extended states are brought about by rotation along the $\bar{4}$ axis. Data from the high temperature structural analysis of

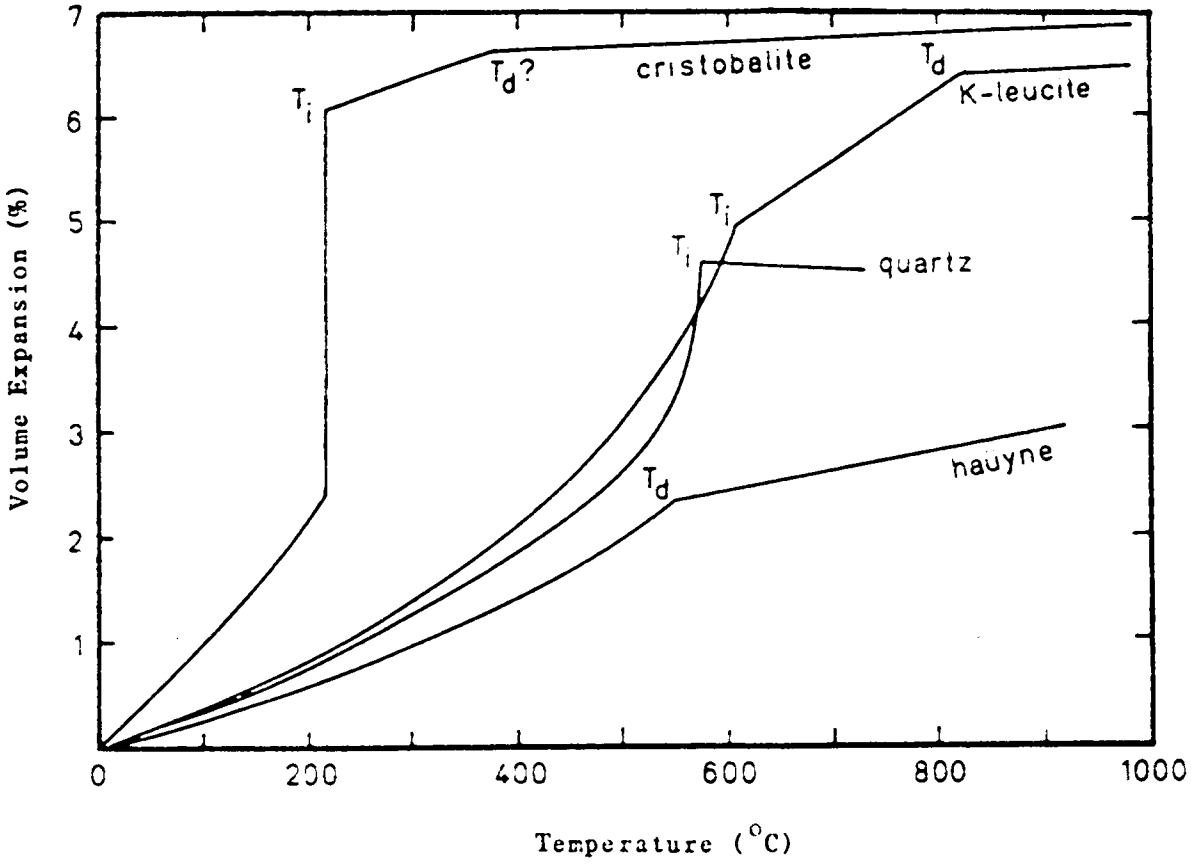

Figure 9. Thermal expansion of framework silicates showing different stages of expansion. T_i is the inversion temperature and T_d is the discontinuity temperature (ref. 39).

cristobalite prove to support the aforementioned thermal expansion behavior. The Si-O-Si angle of low cristobalite measured by Smith and Fable[21] showed a large increase from 146.70° at 23°C to 148.45° at 200°C. Above the inversion temperature, the Si-O-Si angle still showed a slight increase from 147.70° at 221°C to 148.90° at 310°C according to Peacor's single crystal study, or from 146.70° at 300°C to 148.40° at 500°C based on Wright and Leadbetter's results. Table 2 summaries the bond length and bond angle changes of cristobalite with temperatures.

The current studies consider (1) the effects of cation substitutions on the high-low inversion of cristobalite, and (2) the stabilization of high cristobalite. The inversion temperature of cristobalite was investigated by incorporating Ti, Al, B, and P into the high cristobalite phase. The maximum solubility of TiO_2, $AlPO_4$, and BPO_4 in high cristobalite was determined, and the respective phase diagrams at the high silica corner were constructed. The formation and stabilization mechanisms of high cristobalite were studied using sol-gel processing. The thermal expansion and stability of high cristobalite were also tested.

Table. 2 Interatomic Distances and Angles of High Cristobalite (from ref. 15,27)

Temp. (^{o}C)	Si-O (A)	Si-O-Si (^{o})
221[a]	1.615	147.7
248[a]	1.613	148.3
273[a]	1.614	148.0
310[a]	1.611	148.9
400[b]	1.611	147.0
500[b]	1.607	148.4
600[b]	1.609	148.0
700[b]	1.608	148.3
800[b]	1.609	148.1
900[b]	1.609	148.1
1000[b]	1.611	147.7
1200[b]	1.609	148.

Data marked with a and b are taken from ref. 15 and 27, respectively.

II. Experimental Procedure

A. Processing

1. Solid state reaction

Samples used for the inversion temperature studies were prepared by solid state reaction. Reagent-grade chemicals shown in Table. 3 were used as raw materials. Compounds which possess the derivative structure of cristobalite were first synthesized. $AlPO_4$ and BPO_4 were prepared by mixing $Al(OH)_3 \cdot xH_2O$ or H_3BO_3 with $(NH_4)H_2PO_4$ in acetone and firing in platinum crucible at 1250°C for 72 hours and 1050°C for 40 hours, respectively. A slow heating rate is necessary in order to avoid phosphorus loss. $CsLiWO_4$ and $CsLiMoO_4$ were synthesized by mixing Cs_2CO_3, Li_2CO_3, and either WO_3 or MoO_3 according to the 1:1:2 molar ratio. The mixtures were fired in platinum crucibles at 900°C for 3 hours. X-ray examination of the synthesized compounds showed single phases and good crystallinity. Silicic acid was mixed with the respective compounds to form compositions in the systems, SiO_2-TiO_2, SiO_2-$AlPO_4$, SiO_2-BPO_4, SiO_2-$AlPO_4$-TiO_2, SiO_2-BPO_4-TiO_2, and SiO_2-$AlPO_4$-BPO_4. Repeated mixing and grinding in acetone were employed to achieve composition homogeneity and also to reduce particle size. The mixtures containing either $AlPO_4$ or BPO_4 were calcined first, and then sealed in platinum tubes to ensure composition control during heat treatments. The compositions prepared for the SiO_2-TiO_2, SiO_2-$CsLiMoO_4$, and SiO_2-$CsLiWO_4$ systems were directly fired in air. A heat treatment of 72 hours was used for all the compositions. Samples

Table 3. Raw Materials Used in Solid-State Reaction.

$Al(OH)_3 \cdot nH_2O$, $(NH_4)H_2PO_4$, H_3BO_3,
Cs_2CO_3, Li_2CO_3, MoO_3, WO_3,
$MgCO_3$, $CaCO_3$, TiO_2, silicic acid.

were quenched in cold water at the end of heat treatment, followed by phase analysis and property measurements.

2. Sol-gel synthesis

Sol-gel processing is well documented in the literature.[41-47] The basic principles involve hydrolyzing metal alkoxides in alcoholic solutions and polymerizing the hydrolyzed sol to form a gel. The gel is formed by extensive cross-linking or entangling of the long chain molecules. The net reactions to form the anhydrous oxides are generally expressed as:

$$M(OR)_n + xH_2O \longrightarrow M(OH)_x(OR)_{n-x} + xROH \quad (1)$$

$$M(OH)_x(OR)_{n-x} \longrightarrow MO_{n/2} + (x/2)H_2O + (n-x)/2R_2O \quad (2)$$

where M and R represent metal ion and alkyl group, respectively. In reaction (1) the molar ratio of the water added for hydrolysis to the alkoxide ranges from one to over 20. The hydrolysis and condensation reactions are usually catalyzed by the addition of acid or base. The processing temperature at which the reactions take place varies from room temperature to 80°C.

In the present study, the reagent-grade precursors shown in Table 4 were used to synthesize high cristobalite. The precursors consist of metal alkoxides and various salts. Sample compositions were prepared according to the chemical formula $MO \cdot Al_2O_3 \cdot xSiO_2$, where M = Mg, Ca, Sr, Ba, Zn, Fe, Cu, Ni, Pb, and Sn, and x is between 2 and 70. Compositions were also prepared by substituting B, P, and Ti for Al and Si. The precursors were weighed and mixed in ethyl alcohol and deionized water was added to hydrolyze the alkoxides. The molar ratio of water to the framework cations varied from 2 to 10. The hydrolysis

Table 4. Precursors Used in Sol-Gel processing.

Inerstitial cation	Framework cation
$Ca(O_2C_3H_5)_2$, $Ca(NO_3)_2 \cdot 4H_2O$, $Mg(OC_2H_5)_2$, $Mg(NO_3)_2 \cdot 6H_2O$, $SrCl_2 \cdot 6H_2O$, $Ba(OH_3CO_2)_2$, $Zn(NO_3)_2 \cdot 6H_2O$, $FeCl_2 \cdot 4H_2O$, $CuCl_2 \cdot 2H_2O$, $Ni(NO_3)_2 \cdot 6H_2O$, $Pb(NO_3)_2$, $SnCl_2 \cdot 2H_2O$.	$Al(OC_4H_9)_3$, $Al(NO_3) \cdot 9H_2O$, $Si(OC_2H_5)_4$, $(C_2H_5O)_3P(O)$, $Ti[OCH(CH_3)_2]_4$, H_3BO_3.

and condensation reactions were carried out under both acid and base catalyzed conditions. Depending on the pH value, gels resulted in less than 10 hours after the solutions were allowed to stand at ambient temperature. The gel samples were dried between 60 and 70°C for two days, and then gradually heated to 1000°C for 24 hours.

B. Characterization

1. Phase analysis

Standard XRD analyses were performed on all samples using Cu target with K_{α} = 1.542 A. The system was calibrated using a silicon standard and a scanning rate of approximately 1°/min. The presence of a glassy phase was determined by using a polarizing microscope.

2. Thermal analysis

The high-low inversion temperature of cristobalite was determined by differential scanning calorimetry (DSC) at a scanning rate of 20°C/min. The temperature and reaction heat effect were calibrated using pure indium and zinc metals. The peak temperature was taken as the inversion temperature of cristobalite, instead of the onset temperature, since the inversion peak is actually made up of inversions from individual cryatallites in the sample. The gel behaviors upon heating were characterized by differential thermal analysis (DTA), and thermogravimetric analysis (TGA) at a heating rate of 20°C/min. The DTA temperature and reaction heat effect were calibrated by using a gold standard.

3. Chemical analysis

Chemical analysis was performed on selected samples prepared by the sol-gel method to ensure the composition remained constant during the processing and subsequent heat treatments. The samples were examined by Energy Dispersive X-ray (EDX) at an operating voltage of 30 kv.

4. Thermal expansion measurement

Coefficient of thermal expansion was measured using a dual push rod dilatometer with Al_2O_3 as a reference. Sapphire crystals were used to correct system errors. Samples with dimensions of 25 mm in length and 5 mm in diameter were measured using a heating rate of $10^{o}C$/min. Axial thermal expansion was also determined for stabilized high cristobalite using high temperature x-ray diffraction and platinum as an internal standard.

5. Spectroscopic analysis

Raman and fast Fourier Transform Infrared Spectroscopy (FTIR) were used to study the structural changes that occurred as the gel converted to crystalline phase. The gels were heated at 200, 400, 600, 800, and $1000^{o}C$ for 2 hours each. The KBr pellets used for FTIR analysis were prepared by mixing KBr with the pulverized sample in a 400 : 1 weight ratio. The mixture was pressed at 25,000 psi to form a transparent disc with dimensions of 12.5 mm in diameter and 1 mm in thickness. Powder samples were directly used for Raman analysis. The Raman spectrometer was calibrated using the frequency of mercury light, while FTIR was internally calibrated to a resolution of 4 cm^{-1}.

III. Results and Discussion

A. Inversion Temperature of Cristobalite Solid Solution

1. The SiO_2-TiO_2 system

Published information describing the phase relations in the SiO_2-TiO_2 system presents varying experimental observations.[48-50] Uncertainties in this system include the solubility limits at both ends of the system and the eutectic composition. However, only the high silica portion of the system is of concern in this study.

Table 5 shows the compositions studied and the heat treatment temperatures. Standard XRD and petrographic analyses were conducted on each sample after a 72 hour heat treatment. The phases obtained as well as the inversion temperatures of cristobalite are also listed in Table 5. Mechanical mixtures of α-cristobalite and rutile at different weight ratios were prepared for XRD examination. It was found that the minimum rutile content that can be detected by XRD is slightly greater than 1 wt%. The eutectic composition is located at about 10 % TiO_2 at 1535°C as shown in Fig. 10. The solubility of TiO_2 in SiO_2 appears to be less than 5%. The limited solubility can be attributed to the difference in the ionic sizes, and, perhaps more importantly, to the structural differences between TiO_2 and SiO_2. The rutile structure consists of edge-shared Ti octahedra, while all the Si atoms in cristobalite assume a 4-fold coordination. Therefore, only limited solid solution was formed.

Despite the limited solid solution range, the inversion

Table 5. Phase Analysis and Inversion Temperature of Cristobalite Solid Solution in the SiO_2-TiO_2 System.

Comp. (wt%) SiO_2	Comp. (wt%) TiO_2	Temp.(°C)	Phase present	Inversion temp.(°C)
97	3	1630	α-crist(ss), glass	223
		1525	α-crist(ss)	221
		1450	α-crist(ss)	220
95	5	1630	α-crist(ss), glass	191
		1535	α-crist(ss)	190
		1450	α-crist(ss), rutile(tr)	190
92	8	1630	α-crist(ss), glass	195
		1535	α-crist(ss), glass	190
		1450	α-crist(ss), rutile	192
90	10	1630	glass	---
		1535	α-crist(ss), glass, rutile	191
		1450	α-crist(ss). rutile	195
88	12	1630	glass	---
		1535	α-crist(ss), glass, rutile	190
		1450	α-crist(ss), rutile	192
85	15	1630	rutile, glass	---
		1535	α-crist(ss), rutile, glass	190
		1450	α-crist(ss), rutile	190
80	20	1630	rutile, glass	---
		1535	α-crist(ss), rutile	192
		1450	α-crist(ss), rutile	196

crist = cristobalite, ss = solid solution, and tr = trace.

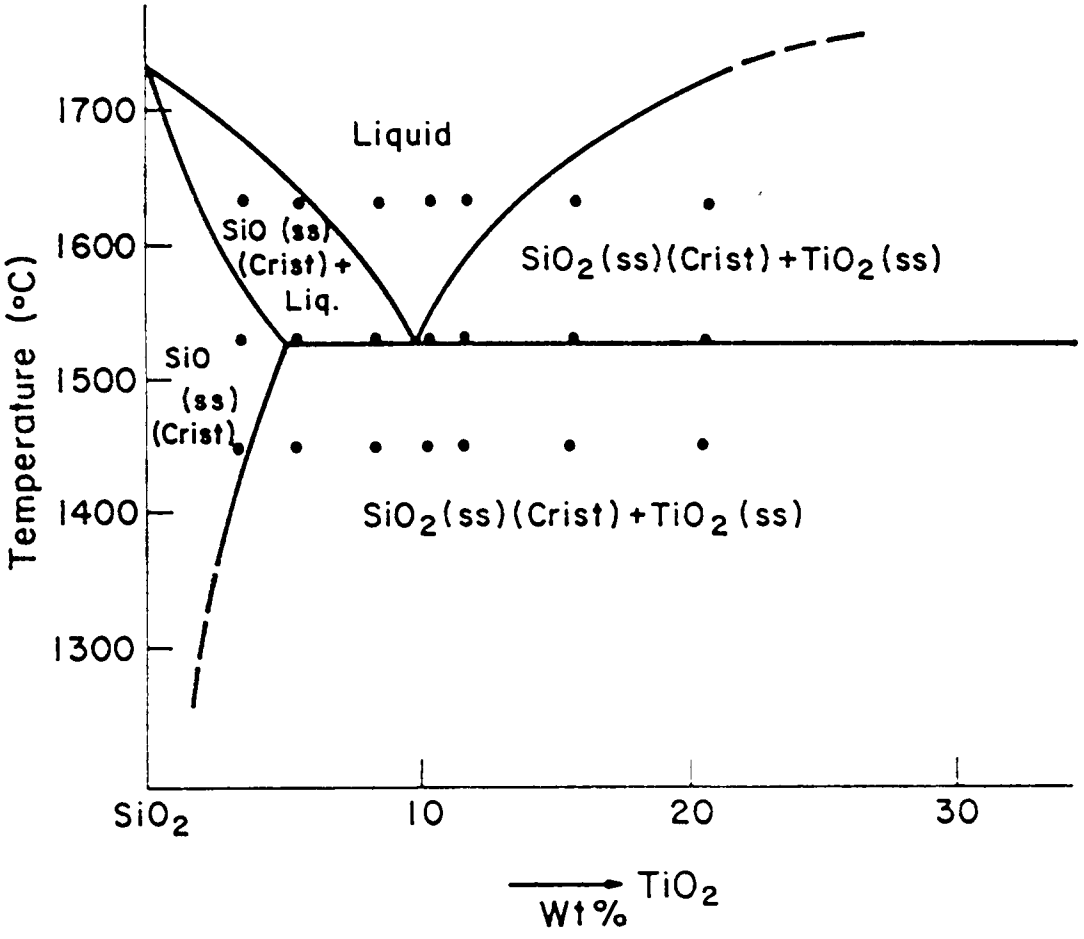

Figure 10. Phase diagram of the high silica region for the SiO_2-TiO_2 system.

temperature of cristobalite can be lowered from 265°C for pure cristobalite to 190°C when Si^{+4} is partially replaced by Ti^{+4}. The presence of Ti^{+4} in cristobalite may cause more disorder, and therefore lowers the inversion temperature. The fact that the inversion temperature ceased to change beyond 5% TiO_2 confirms that the solubility limit cannot be greater than 5 wt%.

2. The SiO_2-$AlPO_4$ System

Phase identification for this system was largely based on petrographic and DSC analyses. Because of the similarities in the XRD patterns, it becomes difficult to separate the cristobalite phases of SiO_2 and $AlPO_4$ by XRD techniques when only a small amount of $AlPO_4$ is present. Nevertheless, these two phases appear to be more discernible under petrographic examination in that the cristobalite phase of $AlPO_4$ shows a higher relief than SiO_2 cristobalite. In addition, the $AlPO_4$ cristobalite phase has a high-low inversion around 210°C, while the high-low inversion for pure SiO_2 cristobalite is generally above 250°C.

Phase analyses for compositions heated at various temperatures are listed in Table 6. The studies concentrate on the SiO_2 cristobalite solid solution range. All compositions were sealed in platinum tubes and quenched in cold water upon the completion of heat treatment. The quenched tubes were visually examined for the presence of leaks. Heat treatments were repeated when cracks were observed. For the temperature and composition range studied, the system appears to contain a binary eutectic as shown in Figure 11. The solubility limit of $AlPO_4$ in SiO_2 is approximately 15% at 1605°C. Results from

Table 6. Phase Analysis and Inversion Temperature of Cristobalite Solid Solution in the SiO_2-$AlPO_4$ System.

Comp. (wt%) SiO_2	$AlPO_4$	Temp.(°C)	Phase	Inversion Temp.(°C)
95	5	1620	α-crist(ss)	244
		1605	α-crist(ss)	243
		1480	α-crist(ss)	244
		1450	α-crist(ss)	244
		1415	α-crist(ss)	247
90	10	1620	α-crist(ss), glass (tr)	246
		1605	α-crist(ss)	245
		1480	α-crist(ss)	247
		1450	α-crist(ss), $AlPO_4$(ss)	246
		1415	α-crist(ss), $AlPO_4$(ss)	245
85	15	1620	α-crist(ss), glass	248
		1605	α-crist(ss)	248
		1480	α-crist(ss), $AlPO_4$(ss)	247
		1450	α-crist(ss), $AlPO_4$(ss)	247
		1415	α-crist(ss), $AlPO_4$(ss)	250
82	18	1620	α-crist(ss), glass	247
		1605	α-crist(ss), glass	249
		1480	α-crist(ss), $AlPO_4$(ss)	247
		1450	α-crist(ss), $AlPO_4$(ss)	248
		1415	α-crist(ss), $AlPO_4$(ss)	246
79	21	1620	α-crist(ss), glass	249
		1605	α-crist(ss), glass	247
		1480	α-crist(ss), $AlPO_4$(ss)	245
		1450	α-crist(ss), $AlPO_4$(ss)	248
		1415	α-crist(ss), $AlPO_4$(ss)	248

Table 6. (continued)

75	25	1650	α-crist(ss) (tr), glasss	---
		1590	α-crist(ss), $AlPO_4$(ss)	247
		1480	α-crist(ss), $AlPO_4$(ss)	245
70	30	1650	α-crist(ss)(tr), glass	---
		1590	α-crist(ss), $AlPO_4$(ss)	247
		1480	α-crist(ss), $AlPO_4$(ss)	246
60	40	1650	$AlPO_4$(ss), glass	---
		1590	α-crist(ss), $AlPO_4$(ss)	247
		1480	α-crist(ss), $AlPO_4$(ss)	246

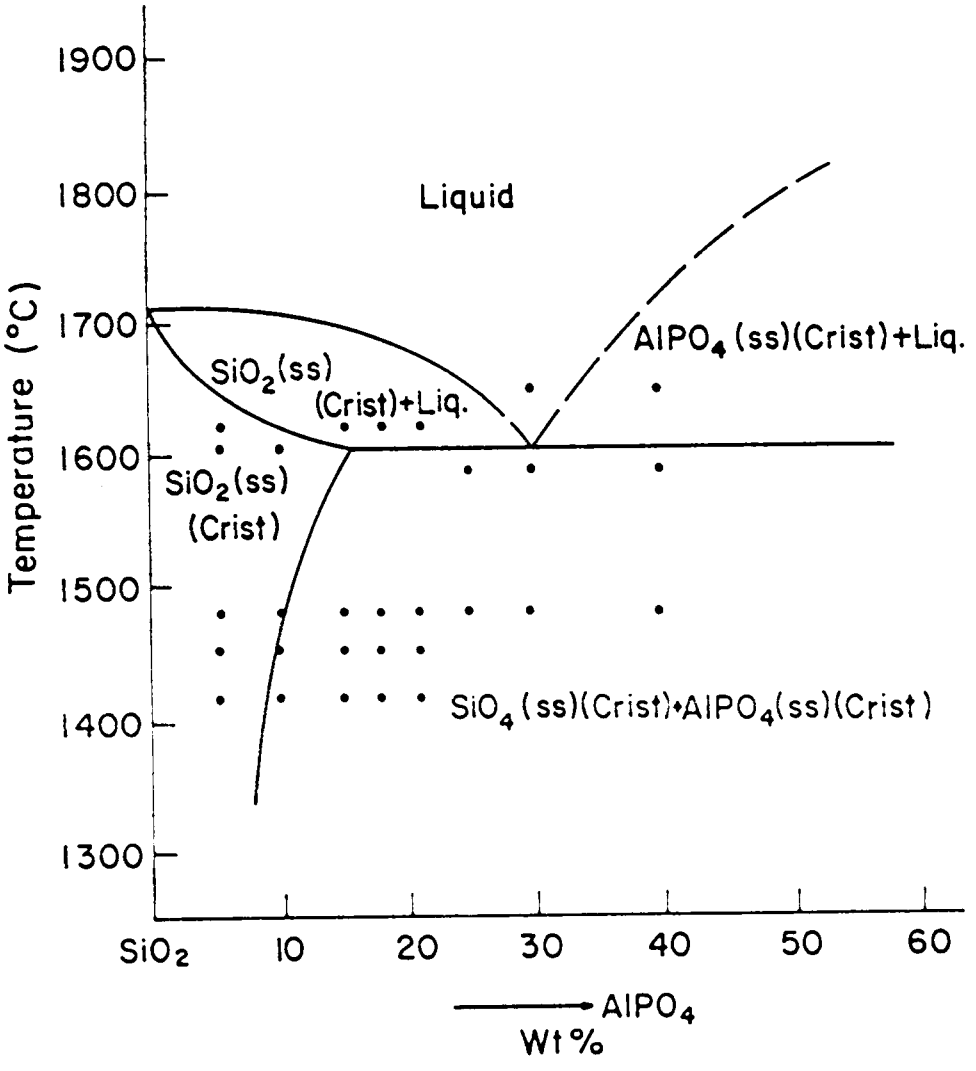

Figure 11. Phase diagram of the high silica region for the SiO_2-$AlPO_4$ system.

other studies showed that the eutectic temperature is at about 1420°C.[51] However, the liquid phase was not observed even at 1590°C for samples prepared in the present study. The last three compositions in Table 6 were used to check the eutectic temperature, although their $AlPO_4$ content is far beyond the solid solution range. Results showed that the eutectic temperature is between 1590 and 1650°C. Based on the formation of liquid phase, the eutectic temperature is located at 1605°C.

The inversion temperatures of SiO_2 cristobalite solid solution are also listed in Table 6. The presence of $AlPO_4$ does not appear to be effective in lowering the inversion temperature despite the fact that the solid solution range is much larger than that of the SiO_2-TiO_2 system. The high-low inversion parameters of cristobalite solid solution at different $AlPO_4$ contents are shown in Table 7. The enthalpy and entropy differences of the $AlPO_4$-modified cristobalite were reduced when compared to those of pure cristobalite.

3. The SiO_2-BPO_4 System

Phase analyses of the heat-treated samples are shown in Table 8. The SiO_2-BPO_4 system appears to be a binary eutectic as shown in Fig. 12. The solubility limit of BPO_4 in SiO_2 is 10% at 980°C. Because of the low melting temperature of BPO_4, the eutectic temperature of the SiO_2-BPO_4 system is much lower than those determined for the SiO_2-TiO_2 and SiO_2-$AlPO_4$ system. The results were further verified by doubling the heat treatment time for all the compositions.

The inversion temperature of the BPO_4-modified cristobalite shows

Table 7. Transformation Parameters of Cristobalite Solid Solution in the SiO_2-$AlPO_4$ Ststem.

Comp (wt%) SiO_2	$AlPO_4$	Temp. (° C)	$T_{\alpha\beta}$ (° C)	$\Delta H_{\alpha\beta}$ (J/g)	$\Delta S_{\alpha\beta}$ (J/g·K)
95	5	1605	243	8.33	0.016
90	10	1605	245	11.21	0.022
85	15	1605	248	7.86	0.015
100		1605	269	19.89	0.037

Table 8. Phase Analysis and Inversion Temperature of Cristobalite Solid Solution in the SiO_2-BPO_4 System.

Comp. (wt%) SiO_2	Comp. (wt%) BPO_4	Temp. (°C)	Phase	Inversion Temp. (°C)
97	3	1020	α-crist(ss)	235
		1000	α-crist(ss)	229
		980	α-crist(ss)	226
		940	α-crist(ss)	227
93	7	1020	α-crist(ss), glass(tr)	187
		1000	α-crist(ss), glass(tr)	185
		980	α-crist(ss)	184
		940	α-crist(ss)	184
90	10	1020	α-crist(ss), glass	190
		1000	α-crist(ss), glass(tr)	189
		980	α-crist(ss)	183
		940	α-crist(ss), BPO_4(ss)	184
88	12	1000	α-crist(ss), glass	186
		980	α-crist(ss), glass(tr)	184
		940	α-crist(ss), BPO_4(ss)	185
86	14	1000	α-crist(ss), glass	187
		980	α-crist(ss), glass, BPO_4(ss)	184
		940	α-crist(ss), BPO_4(ss)	184

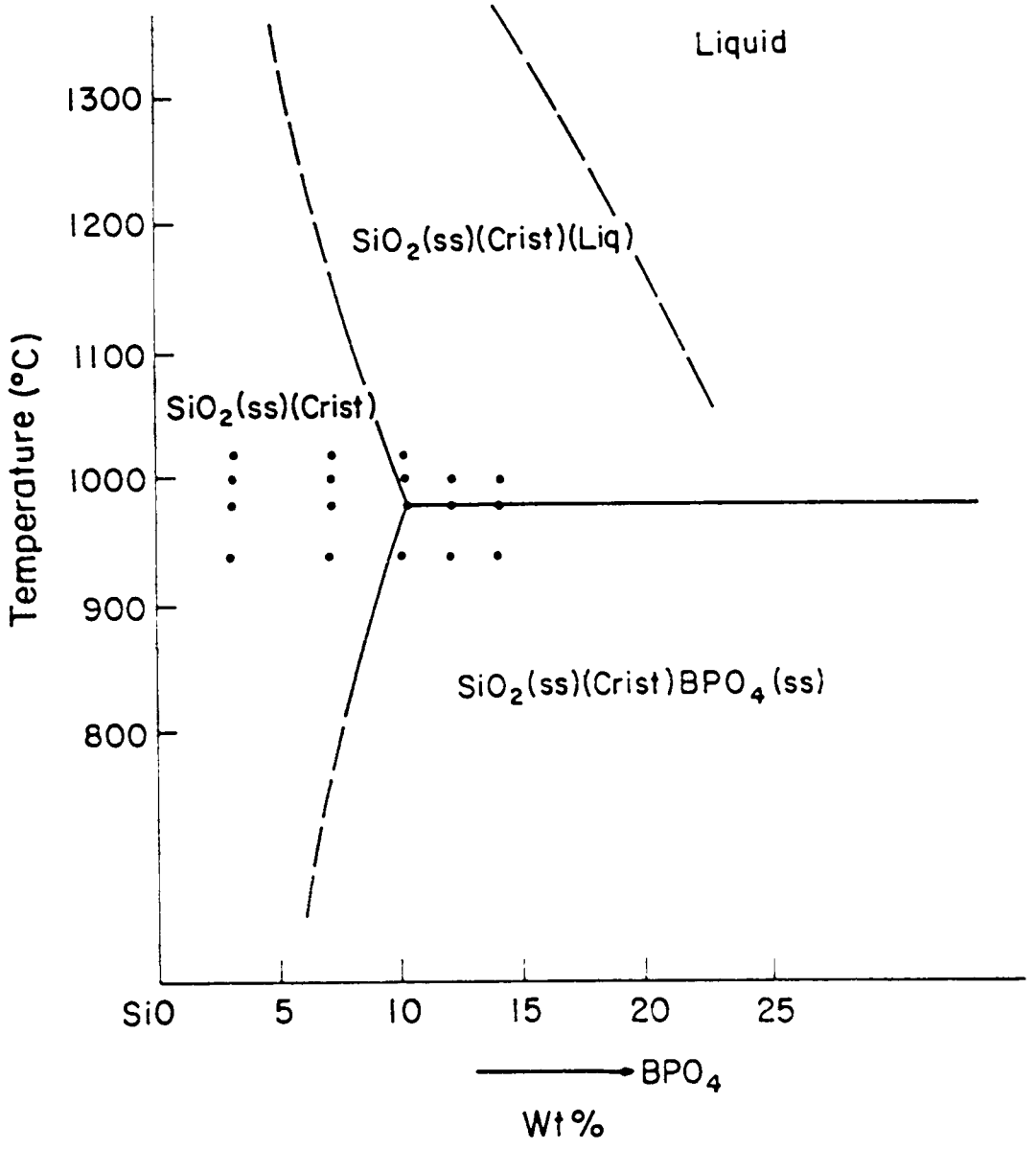

Figure 12. Phase diagram of the high silica region for the SiO_2-BPO_4 system.

a minimum at 183°C for 10% BPO_4 (Table 8). Introducing BPO_4 to the cristobalite lattice also reduces the enthalpy and entropy differences between the high and low temperature phases as shown in Table 9. Of the three binary systems, the BPO_4-modified cristobalite has the lowest inversion temperature; however, its melting temperature is also the lowest.

4. The SiO_2-$AlPO_4$-TiO_2 System

Table 10 lists the phases and inversion temperatures of cristobalite solid solution after heat treatments at different temperatures. Phase analyses of the samples indicate that the SiO_2-$AlPO_4$-TiO_2 system represents a true ternary subsystem of the quarternary system. Fig. 13 shows a portion of the isothermal section of the eutectic plane at 1492°C. The maximum cristobalite solid solution contains approximately 4% TiO_2 and 8% $AlPO_4$ at 1492°C.

The inversion temperatures of cristobalite solid solutions show a continuous decrease with increasing concentration of $AlPO_4$ and TiO_2. The lowest inversion temperature for the SiO_2-$AlPO_4$-TiO_2 system occurs at 162°C. The presence of the second phase does not seem to change the inversion temperature for compositions beyond the solid solution range. It is likely that the lowering of the inversion temperature primarily results from the effect of TiO_2, even though the solubility of $AlPO_4$ is higher. As shown in Table 10, samples with TiO_2 concentrations lower than 5% exhibit relatively high inversion temperatures (above 174°C). On the other hand, when the TiO_2 content is sufficiently high (around 5%), the inversion temperature can be lowered to 162°C with only 3% $AlPO_4$. This is also made clear by the

Table 9. Transformation Parameters of Cristobalite Solid Solution for the SiO_2-BPO_4 System.

Comp. (wt) SiO_2	Comp. (wt) BPO_4	Temp.(°C)	$T_{\alpha\beta}$ (°C)	$\Delta H\alpha\beta$ (J/g)	$\Delta S_{\alpha\beta}$ (J/g·K)
97	3	980	226	16.3	0.033
93	7	980	184	8.58	0.019
90	10	980	183	6.58	0.014

Table 10. Phase Analysis and Inversion Temperature of Cristobalite Solid Solution for the SiO_2 - $AlPO_4$ - TiO_2 System

Composition (wt%)					Inversion
SiO_2	$AlPO_4$	TiO_2	Temp (°C)	Phase	Temp (°C)
93	5	2	1413	α-crist(ss), $AlPO_4$(ss)	196
			1475	α-crist(ss), $AlPO_4$(ss)(tr)	193
			1492	α-crist(ss)	193
			1513	α-crist(ss), glass	194
90	7	3	1413	α-crist(ss), $AlPO_4$(ss)(tr)	184
			1475	α-crist(ss), $AlPO_4$(ss)	180
			1492	α-crist(ss), glass(tr)	185
			1513	α-crist(ss), glass	179
90	5	5	1413	α-crist(ss), TiO_2	192
			1475	α-crist(ss), TiO_2	167
			1492	α-crist(ss)	165
			1513	α-crist(ss), glass	174
90	3	7	1413	α-crist(ss), TiO_2	190
			1475	α-crist(ss), TiO_2	170
			1492	α-crist(ss), TiO_2	162
			1513	α-crist(ss), glass	164
87	10	3	1413	α-crist(ss), $AlPO_4$(ss), TiO_2	196
			1475	α-crist(ss), $AlPO_4$(ss)	179
			1492	α-crist(ss), $AlPO_4$(ss)(tr)	174
			1513	α-crist(ss), glass, $AlPO_4$(ss)	181
80	15	5	1413	α-crist(ss), $AlPO_4$(ss), TiO_2	191
			1475	α-crist(ss), $AlPO_4$(ss), TiO_2	181
			1492	α-crist(ss), $AlPO_4$(ss), TiO_2	163
			1513	α-crist(ss), $AlPO_4$(ss), glass	175

Table 10. (Continued)

80	10	10	1413	α-crist(ss), $AlPO_4$(ss), TiO_2	191
			1475	α-crist(ss), $AlPO_4$(ss), TiO_2	171
			1513	α-crist(ss), $AlPO_4$(ss), glass	168
78	17	5	1413	α-crist(ss), $AlPO_4$(ss), TiO_2	190
			1475	α-crist(ss), $AlPO_4$(ss), TiO_2	180
			1492	α-crist(ss), $AlPO_4$(ss), TiO_2	162
			1513	α-crist(ss), $AlPO_4$(ss), glass	175
78	15	7	1413	α-crist(ss), $AlPO_4$(ss), TiO_2	192
			1475	α-crist(ss), $AlPO_4$(ss), TiO_2	187
			1513	α-crist(ss). $AlPO_4$(ss), glass	173
70	15	15	1413	α-crist(ss), $AlPO_4$(ss), TiO_2	191
			1475	α-crist(ss), $AlPO_4$(ss), TiO_2	173
			1492	glass	---
60	20	20	1413	α-crist(ss), $AlPO_4$(ss), TiO_2	191
			1475	α-crist(ss), $AlPO_4$(ss), TiO_2	174
			1513	glass, TiO_2(tr), $AlPO_4$(ss)(tr)	---

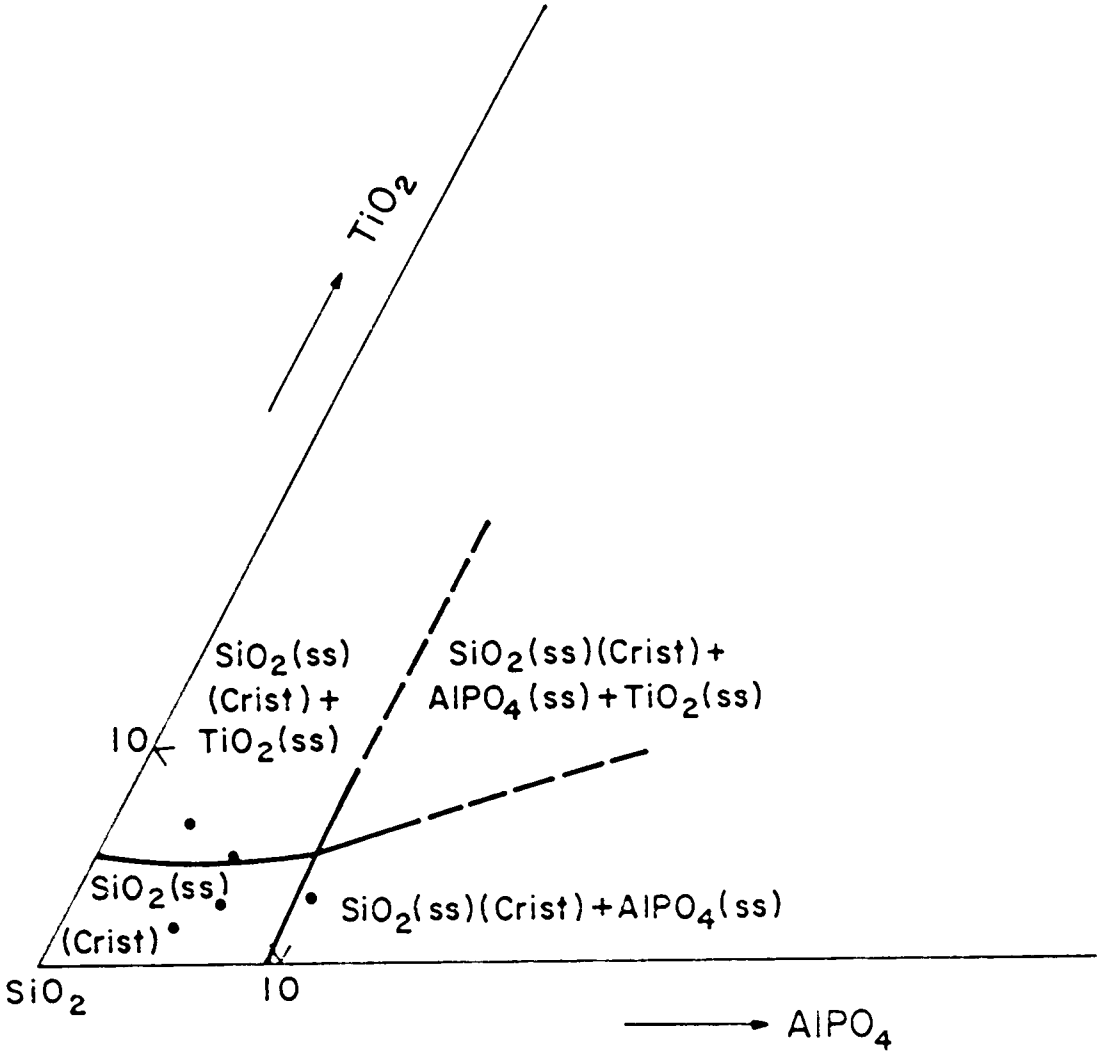

Figure 13. The isothermal section at 1492°C showing the high silica corner of the SiO_2-$AlPO_4$-TiO_2 system.

results obtained from the SiO_2-TiO_2 and SiO_2-$AlPO_4$ system. The inversion temperature can be lowered by 75°C with 5% TiO_2, while 15% $AlPO_4$ only lowers the inversion temperature by 20°C.

5. The SiO_2-BPO_4-TiO_2 System

Phase analysis shows that TiP_2O_7 is present in almost all the compositions studied (Table 11). The results indicate that the SiO_2-BPO_4-TiO_2 system is not a true ternary system, since TiP_2O_7 cannot be expressed in terms of the end members. TiP_2O_7 may have formed from the decomposition of BPO_4 at high temperatures. It was expected that the combined effects of TiO_2 and BPO_4 could further lower the inversion temperature as in the case of the SiO_2-$AlPO_4$-TiO_2 system. Nonetheless, the inversion temperature remains high for the SiO_2-BPO_4-TiO_2 system because TiP_2O_7 formed and consumed both TiO_2 and BPO_4. Therefore, only a limited amount of TiO_2 or BPO_4 can form solid solution with cristobalite. After the formation of TiP_2O_7, the SiO_2-BPO_4-TiO_2 system becomes equivalent to the SiO_2-TiO_2 or SiO_2-BPO_4 system, depending on the compositions. As a result, the inversion temperatures of the SiO_2-BPO_4-TiO_2 system combine characteristics of the SiO_2-BPO_4 system for compositions high in BPO_4 and of the SiO_2-TiO_2 system when excess TiO_2 is present. The inversion temperature cannot be significantly lowered without the simultaneous presence of both TiO_2 and BPO_4 in the cristobalite lattice.

6. The SiO_2-$AlPO_4$-BPO_4 System.

Phase analysis and inversion temperatures are listed in Table 12. The SiO_2-$AlPO_4$-BPO_4 system also appears to be a true ternary system for the composition and temperature range studied. Since $AlPO_4$ and

Table 11. Phase Analysis and Inversion Temperature of Cristobalite Solid Solution for the SiO_2 - BPO_4 - TiO_2 System

Composition (wt%)					Inversion
SiO_2	BPO_4	TiO_2	Temp(°C)	Phase	Temp(°C)
90	7	3	1000	α-crist(ss), TiP_2O_7, B_2O_3	197
			1050	α-crist(ss), TiP_2O_7, glass	201
			1195	α-crist(ss), TiP_2O_7, glass	180
90	5	5	1000	α-crist(ss), TiP_2O_7	193
			1050	α-crist(ss), TiP_2O_7	200
			1195	α-crist(ss), TiP_2O_7	184
90	3	7	1000	α-crist(ss), TiP_2O_7	194
			1050	α-crist(ss), TiP_2O_7	200
			1195	α-crist(ss), TiP_2O_7	222
80	10	10	1000	α-crist(ss), TiP_2O_7, glass	192
			1050	α-crist(ss), TiP_2O_7, glass	201
			1195	α-crist(ss), TiP_2O_7, glass	180
70	15	15	1000	α-crist(ss), TiP_2O_7, glass	193
			1050	α-crist(ss), TiP_2O_7, glass	200
			1195	α-crist(ss)(tr), glass	---

Table 12. Phase Analysis and Inversion Temperature of Cristobalite Solid Solution for the SiO_2-$AlPO_4$-BPO_4 System.

Comp. (wt%) SiO_2	$AlPO_4$	BPO_4	Temp.(°C)	Phase	Inversion Temp.(°C)
90	3	7	1430	glass	---
			1300	α-crist(ss), glass	193
			1160	α-crist(ss), glass	195
			1050	α-crist(ss), glass(tr)	203
90	5	5	1430	α-crist(ss), glass	192
			1300	α-crist(ss), glass	197
			1160	α-crist(ss), BPO_4(ss)(tr)	205
			1050	α-crist(ss)	197
90	7	3	1430	α-crist(ss), glass	239
			1300	α-crist(ss), glass(tr)	238
			1160	α-crist(ss)	226
			1050	α-crist(ss)	219
80	10	10	1430	glass	---
			1300	α-crist(ss), glass	207
			1160	α-crist(ss), glass	196
			1050	α-crist(ss), glass	197

BPO_4 form a complete solid solution series, no invariant plane exists in the SiO_2-$AlPO_4$-BPO_4 system. Similar to the formation of TiP_2O_7, the formation of glassy phase also consumes BPO_4; therefore, only a limited amount of BPO_4 is present in the solid solution. In addition, $AlPO_4$ has little effect on lowering the inversion temperature of cristobalite. As a result, the inversion temperatures obtained for this system are even higher than those of the SiO_2-BPO_4 system.

The inversion temperature of cristobalite was also studied as a function of solid solution with $CsLiWO_4$ and $CsLiMoO_4$, which are structural derivatives of β-cristobalite[52] and which do not show high-low inversions. However, the tridymite phase was formed in most of the compositions because of the mineralizing effect of tungsten and molybdenum oxide.

B. Sol-Gel Synthesis of β-cristobalte

1. Interstitial Cation Substitutions

The compositions studied were prepared using, as a basis, the chemical formula $MO \cdot AlO_3 \cdot XSiO_2$ to form a three dimensional framework silicate linked by the Al and Si tetrahedra. All the oxygen atoms are bridging oxygens and the M ions fit into the interstices to balance the charge. Preliminary studies included most of the divalent cations from the alkaline earth and transition metal group with a wide range of ionic radii. Gel samples were derived from both acid (HNO_3) and base (NH_4OH) catalyzed solutions with H_2O/(Al + Si) molar ratio from 2 to 10. The gels were dried between 60 and 70°C for 2 days followed by

a heat treatment of 1000°C for 24 hours. Table 13 shows the selected compositions and phases formed under the two processing conditions. For base-catalyzed conditions, β-cristobalite was found in the compositions containing Ca, Sr, and Cu, while β-quartz was observed for compositions containing Mg. Results from DSC and DTA analyses further support the fact that both the cristobalite and quartz phases are the high temperature forms since no inversion peak was detected after repeated thermal scanning. On the other hand, an amorphous phase is present in all the acid-catalyzed samples. It is likely that phase separation may have occurred during gelation, resulting in solute-rich and solvent-rich portions. The effect of the $H_2O/(Al+Si)$ ratio on the phase formation was studied by varying the H_2O concentration. No significant difference was observed, except for the gelation time. Based on the preliminary results, the compositions showing the high-temperature phase of either cristobalite or quartz were further studied by varying the SiO_2 content. Since the acid-catalyzed solutions resulted in the formation of the amorphous phase in most cases, the compositional series was prepared under base-catalyzed conditions with a $H_2O/(Al + Si)$ ratio of 4.

$MgO \cdot Al_2O_3 \cdot xSiO_2$ Composition. The compositions studied lie on the SiO_2-$2MgO \cdot 2Al_2O_3 \cdot 5SiO_2$ join of the MgO-Al_2O_3-SiO_2 system. The isoplethal section shown in Fig. 14 indicates that the SiO_2-$2MgO \cdot 2Al_2O_3 \cdot 5SiO_2$ join is not a true binary join because of the presence of mullite. Phase analyses (Table 14) show that β-quartz was stabilized in the Mg-doped compositions. Repeated DTA scanning in the quartz inversion range detected no phase change. The presence of the

Table 13. Preliminary Results form Sol-Gel Synthesis of High Cristobalite.

Composition	Phase Present	
	Base-catalyzed	Acid-catalyzed
$MgO \cdot Al_2O_3 \cdot 30SiO_2$	β-quratz(ss)	amorphous
$MgO \cdot Al_2O_3 \cdot 40SiO_2$	β-quartz(ss)	amorphous
$CaO \cdot Al_2O_3 \cdot 30SiO_2$	β-crist(ss), anorthite	amorphous, anorthite
$CaO \cdot Al_2O_3 \cdot 40SiO_2$	β-crist(ss), anorthite	amorphous, anorthite
$SrO \cdot Al_2O_3 \cdot 30SiO_2$	β-crist(ss), α-crist(ss)	amorphous
$SrO \cdot Al_2O_3 \cdot 40SiO_2$	β-crist(ss), α-crist(ss)	amorphour
$BaO \cdot Al_2O_3 \cdot 30SiO_2$	α-crist(ss), amorphous	amorphous
$BaO \cdot Al_2O_3 \cdot 40SiO_2$	α-crist(ss), amorphous	amorphous
$ZnO \cdot Al_2O_3 \cdot 30SiO_2$	$ZnAl_2O_4$, amorphous	amorphous, $ZnAl_2O_4$
$ZnO \cdot Al_2O_3 \cdot 40SiO_2$	amorphous, $ZnAl_2O_4$	amorphous, $ZnAl_2O_4$
$NiO \cdot Al_2O_3 \cdot 30SiO_2$	amorphous, α-crist(ss)	amorphous
$NiO \cdot Al_2O_3 \cdot 40SiO_2$	amorphous, α-crist(ss)	amorphous
$SnO \cdot Al_2O_3 \cdot 30SiO_2$	SnO_2, amorphous	amorphous, SnO_2
$SnO \cdot Al_2O_3 \cdot 40SiO_2$	SnO_2, amorphous	amorphous, SnO_2
$PbO \cdot Al_2O_3 \cdot 30SiO_2$	α-crist(ss), amorphous	amorphous
$PbO \cdot Al_2O_3 \cdot 40SiO_2$	α-crist(ss), amorphous	amorphous
$CuO \cdot Al_2O_3 \cdot 30SiO_2$	β-crist(ss), α-crist(ss)	amorphous, β-crist
$CuO \cdot Al_2O_3 \cdot 40SiO_2$	β-crist(ss), α-crist(ss)	amorphous, β-crist
$FeO \cdot Al_2O_3 \cdot 30SiO_2$	amorphous, α-crist(ss)	amorphous
$FeO \cdot Al_2O_3 \cdot 40SiO_2$	amorphous, α-crist(ss)	amorphous

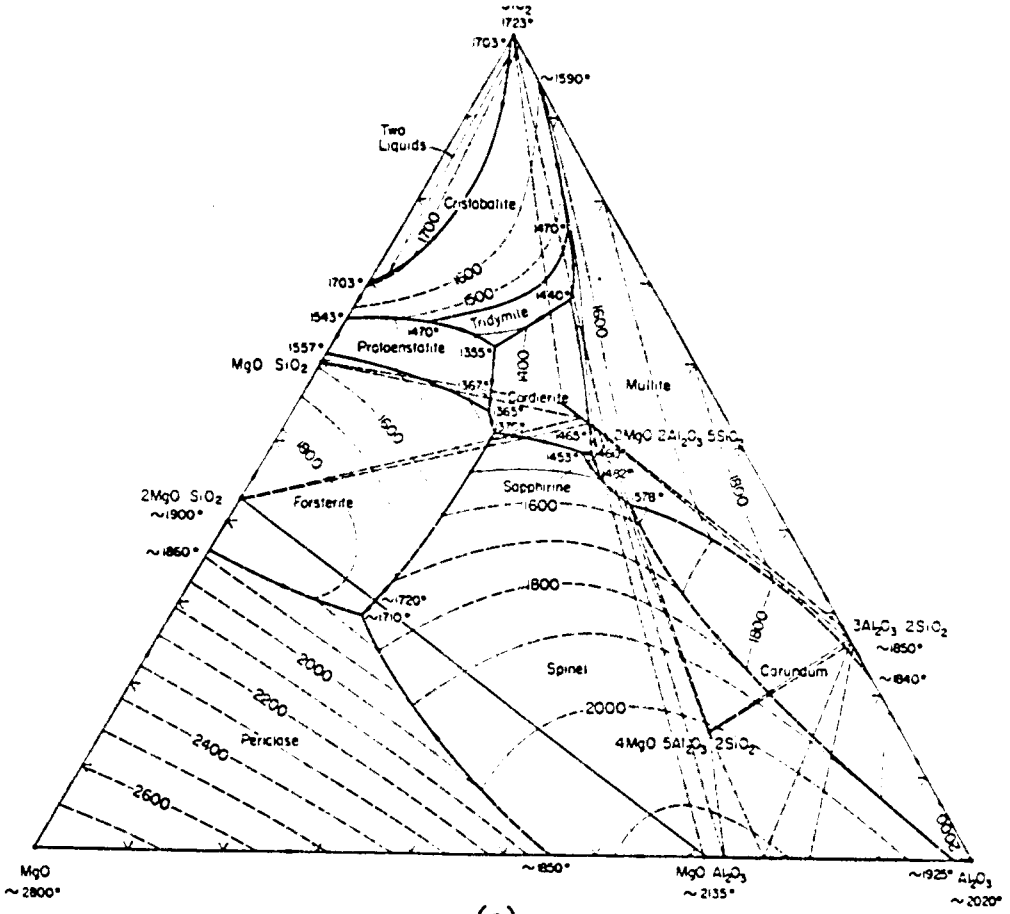

(a)

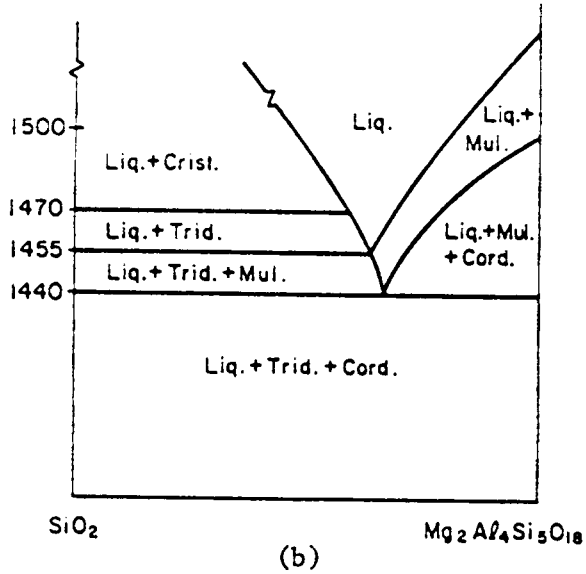

(b)

Figure 14. Phase diagram for the SiO_2-Al_2O_3-MgO system (a) and the isoplethal section of the SiO_2-$2MgO{\cdot}2Al_2O_3{\cdot}5SiO_2$ join (b).

Table 14. Results from Sol-Gel Synthesis for Composition Lying on the SiO_2-$2MgO{\cdot}2Al_2O_3{\cdot}5SiO_2$ Join.

Composition	Phase	CTE α ($10^{-7}/^{\circ}C$)
$2MgO{\cdot}2Al_2O_3{\cdot}5SiO_2$	β-quartz(ss), spinel	----
$MgO{\cdot}Al_2O_3{\cdot}10SiO_2$	β-quartz(ss)	41
$MgO{\cdot}Al_2O_3{\cdot}15SiO_2$	β-quratz(ss)	43
$MgO{\cdot}Al_2O_3{\cdot}20SiO_2$	β-quartz(ss), amorphous	---
$MgO{\cdot}Al_2O_3{\cdot}25SiO_2$	β-quartz(ss), amorphous	---
$MgO{\cdot}Al_2O_3{\cdot}30SiO_2$	β-quartz(ss)	31
$MgO{\cdot}Al_2O_3{\cdot}40SiO_2$	β-quartz(ss)	46
$MgO{\cdot}Al_2O_3{\cdot}50SiO_2$	β-quartz(ss), amorphous	---
$MgO{\cdot}Al_2O_2{\cdot}60SiO_2$	β-quartz(ss), α-quartz(ss)	---

amorphous phase is probably related to incomplete condensation reactions during gel formation. Cordierite ($2MgO \cdot 2Al_2O_3 \cdot 5SiO_2$) was not observed in any of the compositions, including the specimen with a stoichiometric cordierite composition. The phases observed are β-quartz and spinel ($MgO \cdot Al_2O_3$). Compared to the phases predicted by the isoplethal section, the gel-derived phases are apparently metastable. The solubility of ($MgO + Al_2O_3$) in β-quartz appears to be higher than 19 wt% as shown in the $MgO \cdot Al_2O_3 \cdot 10SiO_2$ composition.

The thermal expansion data for compositions containing a single phase are also presented in Table 14. The coefficient of thermal expansion in general decreases with increasing ($MgO + Al_2O_3$) concentration. Fig. 15 shows that the expansion becomes increasingly non-linear as the ($MgO + Al_2O_3$) concentration decreases.

<u>$CaO \cdot Al_2O_3 \cdot xSiO_2$ Composition.</u> The compositions were selected from the SiO_2-$CaO \cdot Al_2O_3 \cdot 2SiO_2$ join. Fig. 16 shows the isoplethal section of the SiO_2-$CaO \cdot Al_2O_3 \cdot 2SiO_2$ join which, unlike the SiO_2-$2MgO \cdot 2Al_2O_3 \cdot 5SiO_2$ join, represents a true binary join. Results from both XRD and DSC measurements (Table 15) show that β-cristobalite was stabilized in all the compositions prepared. Repeated thermal scanning in the cristobalite inversion range revealed no phase transformations. The cristobalite phase is indeed the high temperature phase. The concentration of 5% ($CaO + Al_2O_3$), as in the $CaO \cdot Al_2O_3 \cdot 50SiO_2$ composition, appears to be critical. Above this concentration, anorthite ($CaO \cdot Al_2O_3 \cdot 2SiO_2$) is always present, and either α-quartz or an amorphous phase is formed below the 5% concentration. This also indicates a very limited solubility of CaO and Al_2O_3 in the

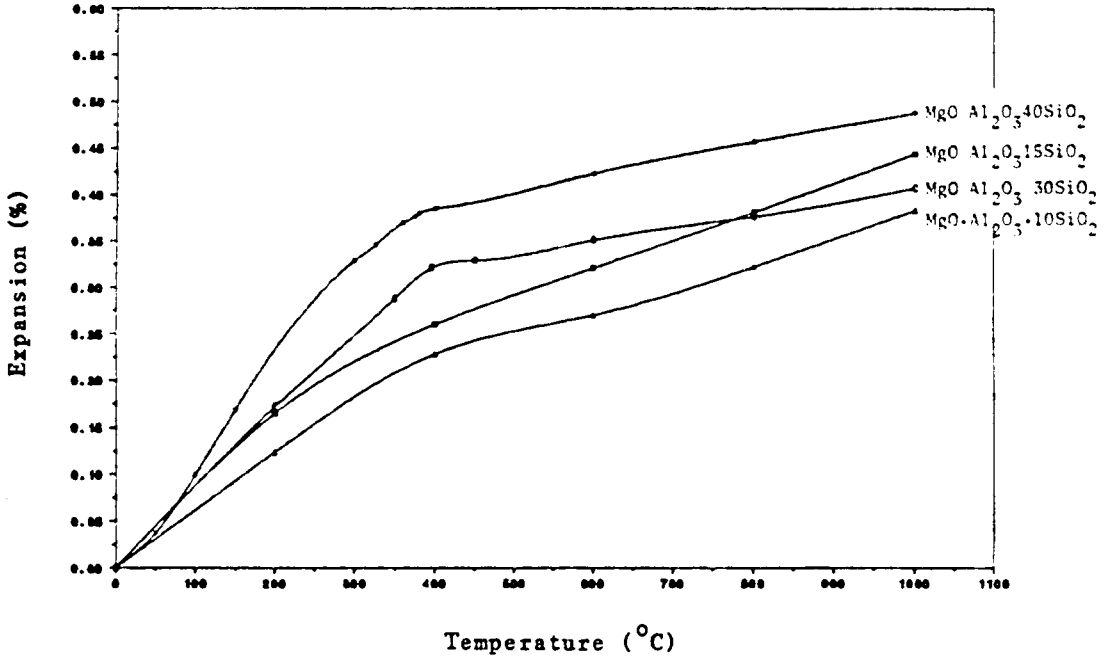

Figure 15. The aggregate thermal expansion of high quartz solid solution for the $MgO \cdot Al_2O_3 \cdot xSiO_2$ compositions.

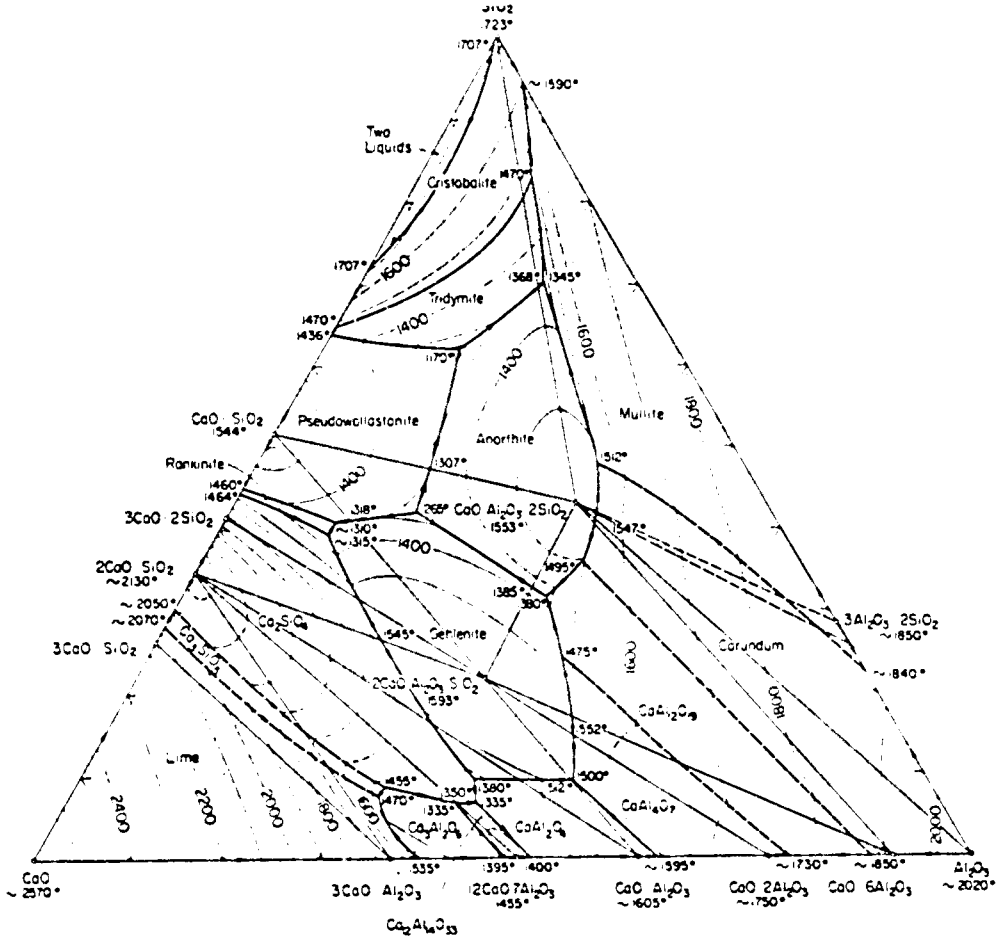

(a)

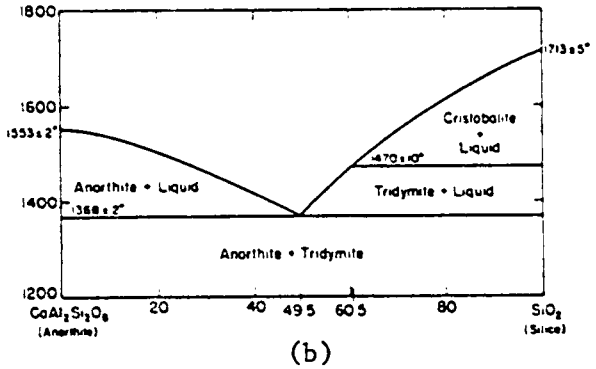

(b)

Figure 16. Phase diagram for the SiO_2-Al_2O_3-CaO system (a) and the isoplethal section of the SiO_2-$CaO{\cdot}Al_2O_3{\cdot}2SiO_2$ join (b).

Table 15. Results from Sol-Gel Synthesis for Compositions Lying on the SiO_2-$CaO \cdot Al_2O_3 \cdot 2SiO_2$.

Composition	Phase
$CaO \cdot Al_2O_3 \cdot 2SiO_2$	anorthite, β-crist(ss)
$CaO \cdot Al_2O_3 \cdot 5SiO_2$	anorthite, β-crist(ss)
$CaO \cdot Al_2O_3 \cdot 10SiO_2$	β-crist(ss), anorthite
$CaO \cdot Al_2O_3 \cdot 15SiO_2$	β-crist(ss), anorthite
$CaO \cdot Al_2O_3 \cdot 20SiO_2$	β-crist(ss), anorthite
$CaO \cdot Al_2O_3 \cdot 25SiO_2$	β-crist(ss), anorthite
$CaO \cdot Al_2O_3 \cdot 30SiO_2$	β-crist(ss), anorthite(tr)
$CaO \cdot Al_2O_3 \cdot 35SiO_2$	β-crist(ss), anorthite(tr)
$CaO \cdot Al_2O_3 \cdot 40SiO_2$	β-crist(ss), anorthite(tr)
$CaO \cdot Al_2O_3 \cdot 50SiO_2$	β-crist(ss), amorphous
$CaO \cdot Al_2O_3 \cdot 60SiO_2$	β-crist(ss), amorphous
$CaO \cdot Al_2O_3 \cdot 70SiO_2$	β-crist(ss), amorphous, α-crist(ss)

cristobalite phase. However, the presence of CaO and Al_2O_3 is necessary to form β-cristobalite at such a low temperature.

The axial thermal expansion of the stabilized β-cristobalite from room temperature to 1000°C is shown in Fig. 17. The observed non-linear expansion implies that the structure still possesses considerable flexibility at low temperatures. This flexibility primarily results from the tilting of the Si-O-Si bond angle, which in turn is associated with the small force constant of the bridging oxygen atom. In contrast to the anticipated results, the thermal expansion of the stabilized β-cristobalite remains high, especially at low temperatures. It is apparent that the bond angle change continues to dominate the thermal expansion of β-cristobalite. Therefore, the lack of a phase transformation does not necessarily ensure low thermal expansion in this case, unless the tilting effect of the bond angle can be eliminated.

$SrO \cdot Al_2O_3 \cdot xSiO_2$ Composition. Phase analysis of these compositions are listed in Table 16. Most of the compositions show the presence of β-cristobalite, except for compositions with low SrO and Al_2O_3 contents. The presence of an amorphous phase can be attributed to incomplete condensation reactions. Therefore the processing was repeated by adjusting the tetraethyl orthosilicate : ethanol : H_2O ratio and also the pH. However, no improvement in the phase formation was observed.

$CuO \cdot Al_2O_3 \cdot xSiO_2$ Composition. Results from phase analyses are listed in Table 17. Except for $CuO \cdot Al_2O_3 \cdot 20SiO_2$, a single phase of β-cristobalite with good crystallinity was observed in the

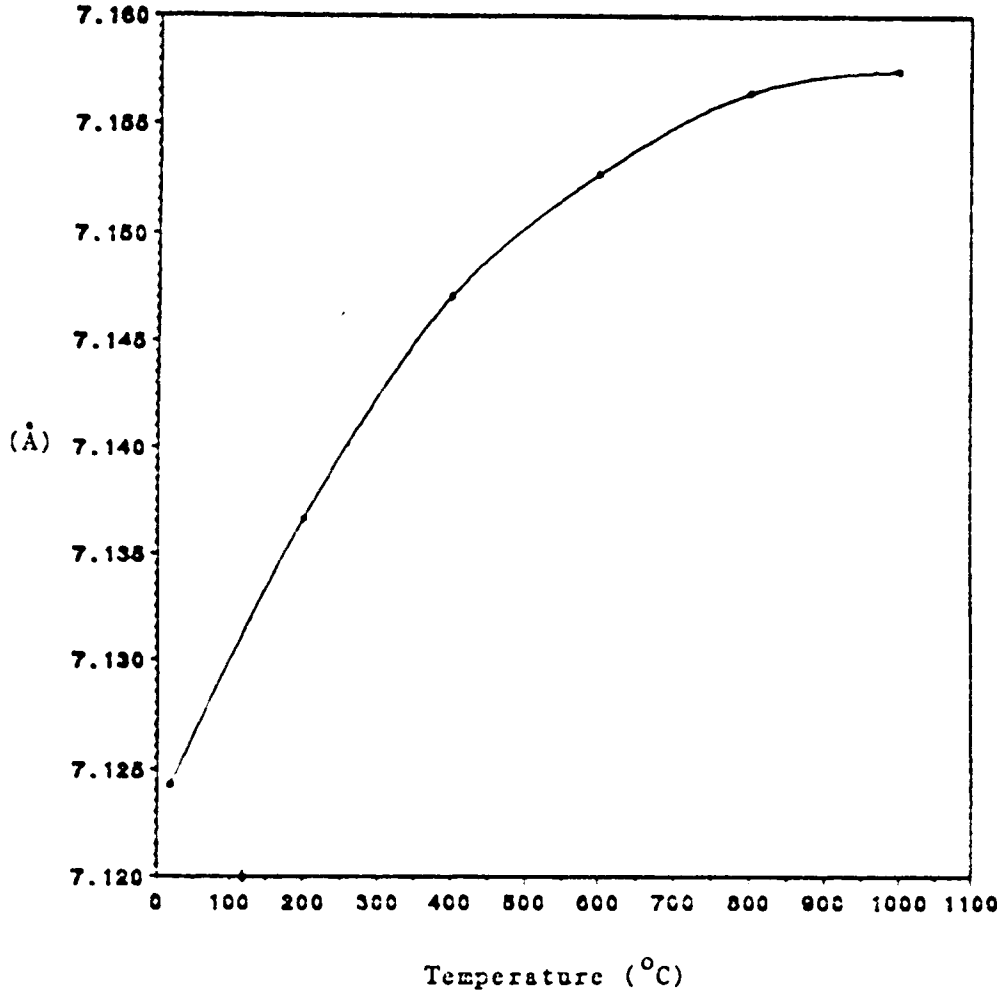

Figure 17. The axial thermal expansion of the Ca-stabilized high cristobalite.

Table 16. Results from Sol-Gel Synthesis for the $SrO \cdot Al_2O_3 \cdot xSiO_2$ Compositions.

Composition	Phase
$SrO \cdot Al_2O_3 \cdot 20SiO_2$	β-crist(ss), amorphous
$SrO \cdot Al_2O_3 \cdot 30SiO_2$	β-crist(ss), amorphous
$SrO \cdot Al_2O_3 \cdot 40SiO_2$	β-crist(ss), amorphous
$SrO \cdot Al_2O_3 \cdot 50SiO_2$	β-crist(ss), α-crist(ss), amorphous
$SrO \cdot Al_2O_3 \cdot 60SiO_2$	α-crist(ss), amorphous

$CuO \cdot Al_2O_3 \cdot xSiO_2$ series of all compositions (Fig. 18). A trace amount of a second phase was observed in the $CuO \cdot Al_2O_3 \cdot 20SiO_2$ composition possibly because of the high concentration of CuO and Al_2O_3. DSC results (Fig. 19) further prove that β-cristobalite is stabilized, since the high-low inversion was not detected. The phase purity of the Cu-stabilized β-cristobalite is significantly better than the Ca- and Sr-stabilized β-cristobalite. However, the CTE values remain high regardless of the Cu content. It seems that the presence of the interstitial cations has little effect on bond angle stretching. Therefore, the thermal expansion behavior of β-cristobalite was examined by performing ionic substitutions on the framework cations, Al and Si.

2. Framework Cation Substitutions

The framework cations of the $CaO \cdot Al_2O_3 \cdot 40SiO_2$ composition were partially replaced by P, Ti, and B, and also by introducing Ca vacancies as shown (Table 18). The hydrolysis and condensation reactions were catalyzed by the addition of NH_4OH with the H_2O/T molar ratio equal to 4, where T represents the framework cations. Results show that anorthite was not observed and pure β-cristobalite was obtained when Si^{+4} was partially replaced by Al^{+3} and P^{+5}. However, part of the β-cristobalite phase transformed to α-cristobalite when the (Al+P) content was increased. Rutile was formed in the Ti-substituted samples because of limited solubility of TiO_2 in cristobalite at the firing temperature. For B-substituted compositions, β-cristobalite completely transformed to α-cristobalite, possibly because of the size effect. Attempts were also made to

Table 17. Results from Sol-Gel Synthesis for the $CuO \cdot Al_2O_3 \cdot xSiO_2$ Compositions.

Composition	Phase	CTE α ($10^{-7}/^{\circ}C$)
$CuO \cdot Al_2O_3 \cdot 20SiO_2$	β-crist(ss), unknown	---
$CuO \cdot Al_2O_3 \cdot 30SiO_2$	β-crist(ss)	75
$CuO \cdot Al_2O_3 \cdot 40SiO_2$	β-crist(ss)	79
$CuO \cdot Al_2O_3 \cdot 50SiO_2$	β-crist(ss)	77
$CuO \cdot Al_2O_3 \cdot 60SiO_2$	β-crist(ss)	78

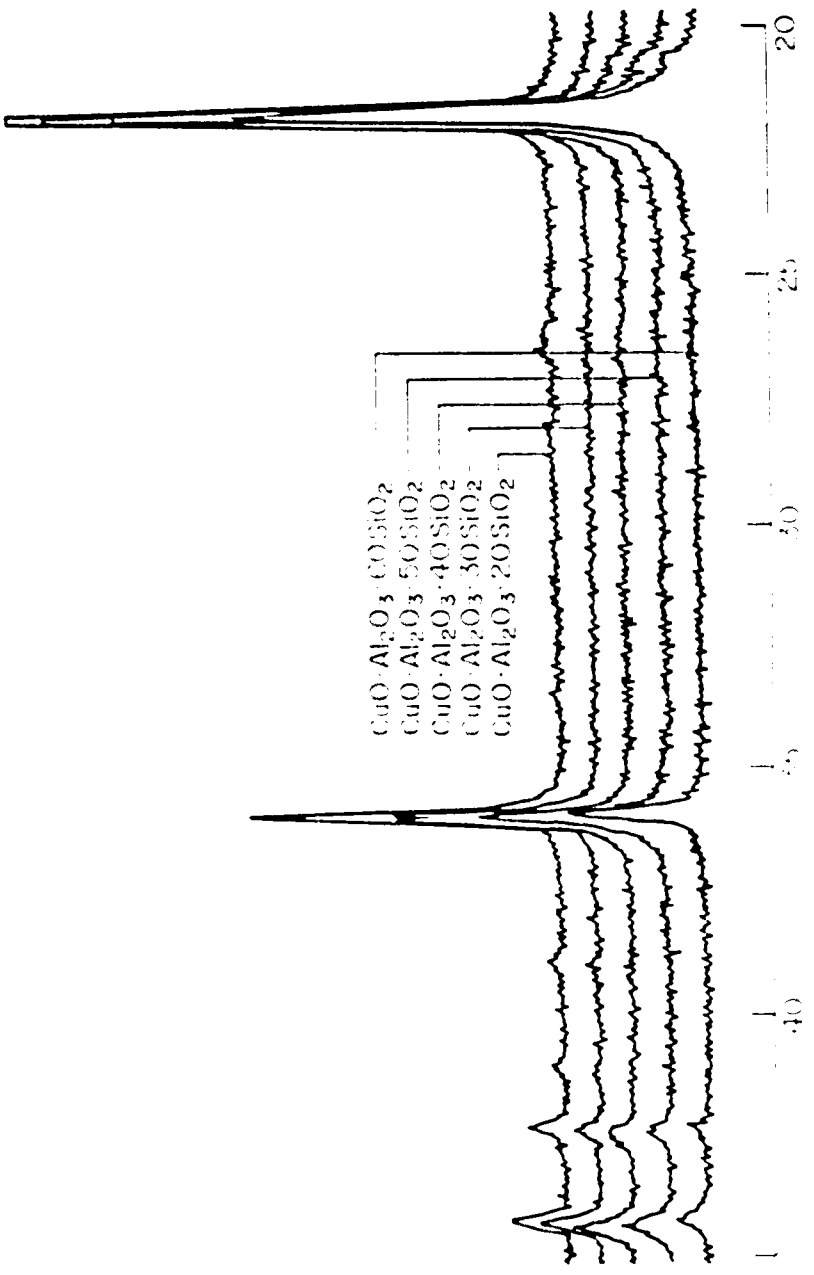

Figure 18. XRD of the $CuO{\cdot}Al_2O_3{\cdot}xSiO_2$ compositions.

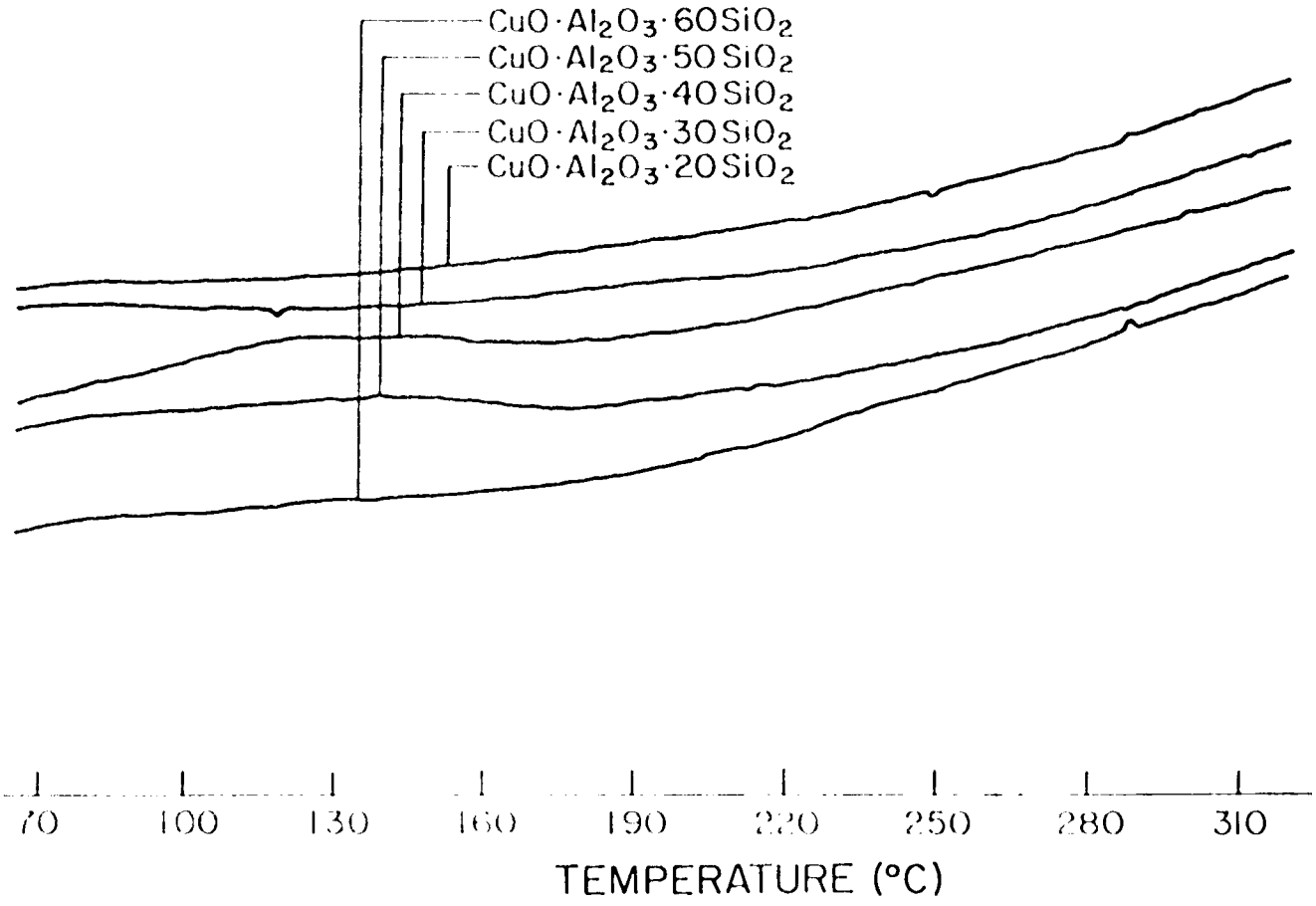

Figure 19. DSC analysis of the Cu-stabilized high cristobalite at a scanning rate of 20°C/min.

Table 18. Phase Analysis and Thermal Expansion for the Compositions Based on Framework Cation Substitutions.

Composition	Phase	Thermal Expansion $\alpha(x10^{-7}/^{o}C)$
$CaAl_2(Si_{38}AlP)O_{84}$	β-cristobalite	75
$CaAl_2(Si_{36}Al_2P_2)O_{84}$	β-cristobalite	86
$CaAl_2(Si_{30}Al_5P_5)O_{84}$	α-, β-cristobalite	--
$CaAl_2(Si_{38}Ti_2)O_{84}$	β-cristobalite, rutile	--
$CaAl_2(Si_{35}Ti_5)O_{84}$	β-cristobalite, rutile	--
$CaAl_2(Si_{30}Ti_{10})O_{84}$	β-cristobalite, rutile	--
$CaB_2Si_{40}O_{84}$	α-cristobalite	--
$CaB_2Si_{30}O_{64}$	α-cristobalite	--
$Ca_{0.8}Al_2(Si_{39.6}P_{0.4})O_{84}$	β-cristobalite	72
$Ca_{0.6}Al_2(Si_{39.2}P_{0.8})O_{84}$	β-cristobalite	83
$Ca_{0.4}Al_2(Si_{38.8}P_{1.2})O_{84}$	β-cristobalite	113
$Ca_{0.2}Al_2(Si_{38.4}P_{1.6})O_{84}$	α-, β-cristobalite	--

stabilize β-cristobalite by decreasing the content of interstitial caitons. It was found that β-cristobalite cannot be completely stabilized without the presence of interstitial cations as shown in the $Ca_{0.2}Al_2(Si_{38.4}P_{1.6})O_{84}$ composition. The coefficient of thermal expansion measured for the single phase is comparable to those determined for the Cu-stabilized β-cristobalite. The species of the framework cations does not seem to affect the thermal expansion of β-cristobalite.

The thermal expansion of framework structures linked by bridging oxygen ions is dominated by the expansion of the framework itself, which appears to be independent of the species of the framework cations as was found in the thermal expansion of leucite[35], and alkali feldspar minerals.[53] The non-linear expansion is generally parallel to the bond angle change. The expansion resulting from the interstitial cations is relatively insignificant when compared to the expansion of the framework. However, the size of the interstitial cation may affect the occurrence of phase transformations. For example, Cs-leucite does not show the cubic-to-tetragonal transformation, which is typical of K-leucite and Rb-leucite. The cubic Cs-leucite also shows significant expansion between room temperature and 200°C, indicating that in the cubic phase the trtrahedra are still tilted. It is perhaps only when the bond angle equals 180° that the tilting effect disappears.

The thermal expansion of stabilized β-cristobalite clearly shows that bond angle tilts still exist. This may not be as evident when the high-low inversion is present. Therefore, it can be said that the

tilting of bond angle is typical for the framework structures. During the tilting, phase transformations may or may not occur depending on whether a new symmetry is generated; in contrast, dimensional changes always result. By the same token, framework structures linked by bridging oxygen ions will normally exhibit high thermal expansion unless their expansion is highly anisotropic as in the case of β-spodumene, β-eucryptite, keatite, β-quartz and cordierite.[54]

3. Phase formation

The formation of β-cristobalite and β-quartz for samples prepared by sol-gel techniques differs considerably from the results predicted by the phase diagram. For example, the phase diagram of the SiO_2-$CaO \cdot Al_2O_3 \cdot 2SiO_2$ system (Fig. 16) predicts that anorthite and tridymite are the equilibrium phases at 1000°C for the $CaO \cdot Al_2O_3 \cdot xSiO_2$ series of composition. The isoplethal section of the SiO_2-$2MgO \cdot 2Al_2O_3 \cdot 5SiO_2$ join (Fig. 14) indicates that cordierite and tridymite should exist for the compositions studied. An amorphous phase is usually found to replace tridymite when SiO_2 is heat treated in the stability region of tridymite. Some of the compositions identical to those prepared by sol-gel methods were prepared by solid state reaction under the same heat treatment conditions, and only an amorphous phase was observed. One possible explanation for the discrepancy between the sol-gel results and the phase diagram is that a eutectoid exists in the SiO_2-$CaO \cdot Al_2O_3 \cdot 2SiO_2$ system and therefore lowers the formation temperature of cristobalite. Likewise, a peritectoid region may be formed in the SiO_2-$2MgO \cdot 2Al_2O_3 \cdot 5SiO_2$ join which extends the stability region of quartz beyond 867°C. However, the limited solid solution

range makes such drastic changes unlikely. Furthermore, it cannot explain why cordierite is not formed in the stoichiometric cordierite composition and β-cristobalite still exists in the stoichiometric composition of anorthite.

It is likely that the formation of the thermodynamically unfavored phase is closely related to the characteristics of the gel. Therefore, the gel behavior upon heating and the structural evolution from the x-ray amorphous gel to its crystalline counterpart was studied. After drying at 65°C for 2 days to remove solvent and H_2O released from condensation reactions, the $CuO \cdot Al_2O_3 \cdot xSiO_2$ series of gels were characterized by DTA and TGA (Figs. 20, 21). The weak endothermic peak shown in the DTA curves is attributed to desorption of physically adsorbed water. The exothermic peak corresponds to the combustion of carbon, assuming that carbon was present only as ethoxide. The presence of ethoxide also indicates that the hydrolysis reaction was not complete in the solution and proceeded at a slower rate than the condensation reaction under the base-catalyzed conditions. The TGA curves show the corresponding weight loss due to the desorption of water around 85-120°C and the combustion of carbon in the vicinity of 220°C, which agrees with the DTA results. A progressively larger weight loss was detected as the SiO_2 content decreased. The small and gradual weight loss above 220°C is probably related to additional condensation reactions.

The structural evolution of the gel sample was examined from 200 to 1000°C using FTIR and Raman spectroscopy. The FTIR spectra for both α-cristobalite and β-cristobalite (Fig. 22) differ in respect to

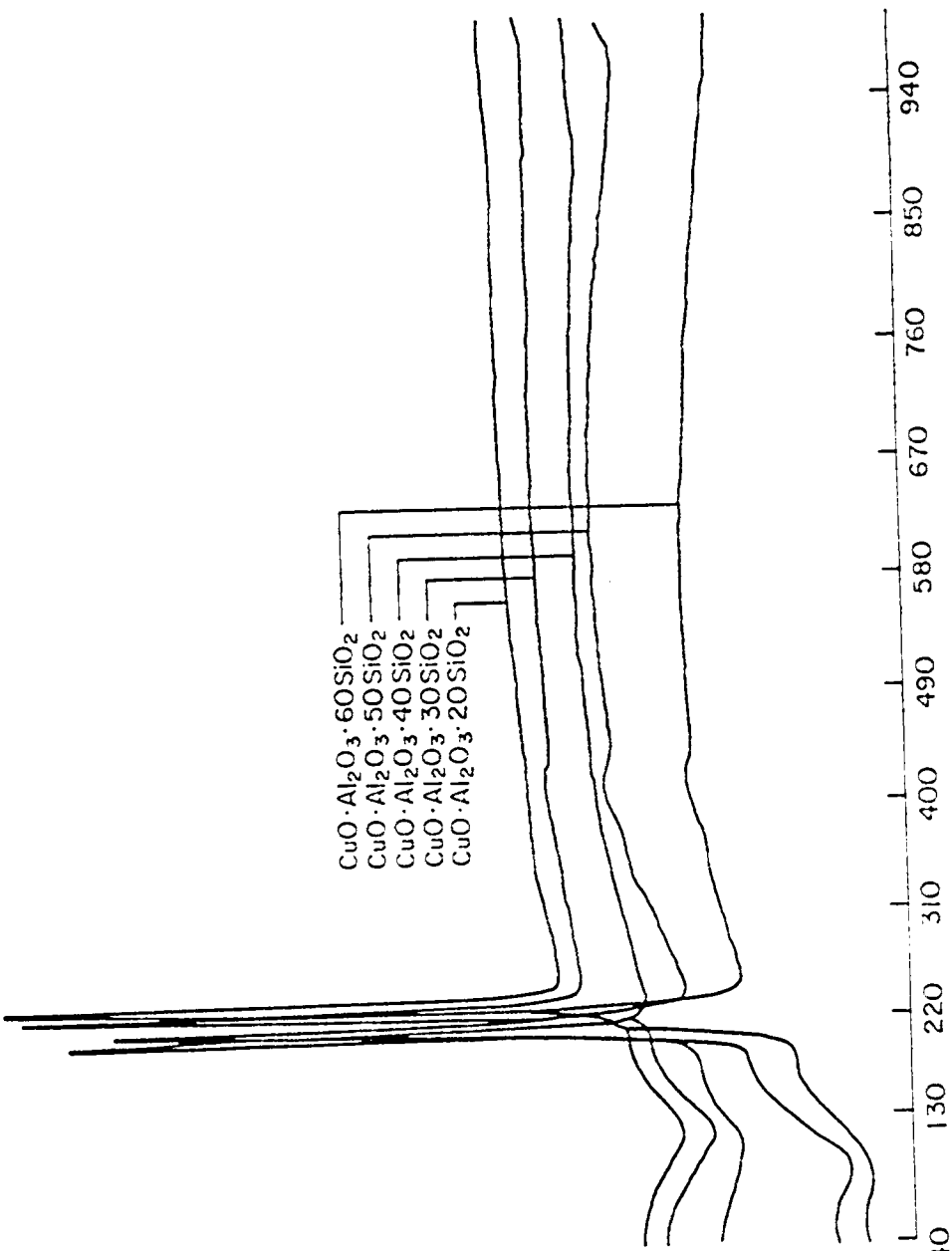

Figure 20. DTA analysis of the gels prepared from the $CuO{\cdot}Al_2O_3{\cdot}xSiO_2$ compositions at a scanning rate of 20°C/min.

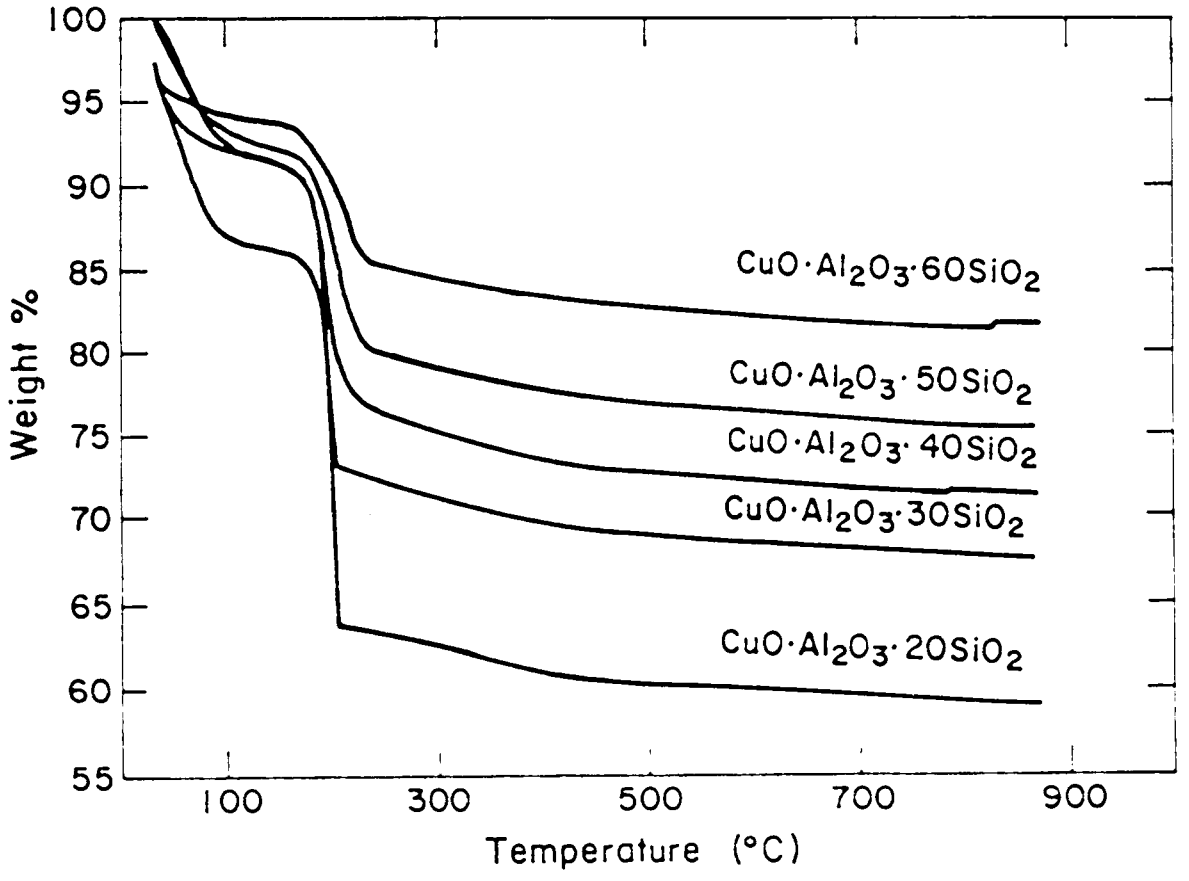

Figure 21. TGA analysis of the gels prepared from the $CuO{\cdot}Al_2O_3{\cdot}xSiO_2$ compositions at 20°C/min.

an absorption peak at 620 cm^{-1}, which appears in α-cristobalite only. Unlike α-cristobalite, β-cristobalite is relatively Raman-inactive. As can be seen in Fig. 23, it is difficult to distinguish between signal and noise for β-cristobalite. Fig. 24 shows the FTIR spectra of both the amorphous gel and the crystalline phase for the $CuO \cdot Al_2O_3 \cdot 30SiO_2$ composition. The absence of the 620 cm^{-1} absorption peak indicates that β-cristobalite was embodied in the local gel structure. The local structure in the xerogel appears to be identical with its crystalline counterpart, except that long range order was not developed at an early stage. Progressive increase in heat treatment times may have increased the ordered region and reduced the unreacted functional group, thereby causing the 1100^{-1} absorption band to become narrower. Prolonged heat treatment at 1000°C eventually results in the complete crystallization of β-cristobalite.

Similar results were found in the formation of the Ca-doped β-cristobalite. The structural evolution from gel to β-cristobalite was also studied for the $CaO \cdot Al_2O_3 \cdot 30SiO_2$ composition (Fig. 25). The FTIR spectra of the amorphous gels are essentially the same as the spectrum of the crystalline phase, indicating that β-cristobalite was formed in the local structure of the xerogels. The only difference between the xerogel and the crystalline phase appears to be the lack of long range order in the xerogels. XRD examinations of the gels heated between 200 and 1000°C show that the long range order was not developed untill 1000°C. Based on the spectra, the formation mechanism of β-cristobalite from the gel precursors seems to be the same for both the $CuO \cdot Al_2O_3 \cdot xSiO_2$ and $CaO \cdot Al_2O_3 \cdot xSiO_2$ compositions.

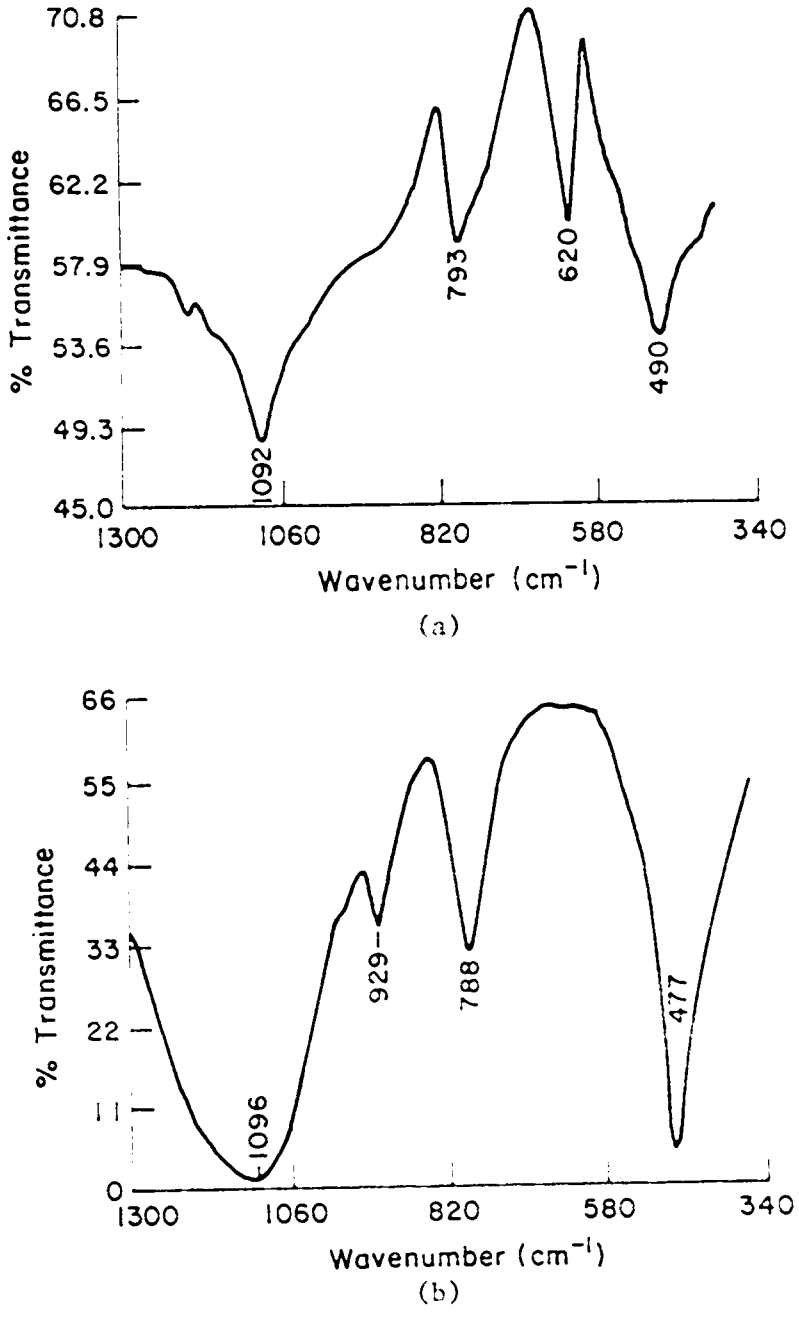

Figure 22. FTIR spectrum for low cristobalite (a) and high cristobalite (b).

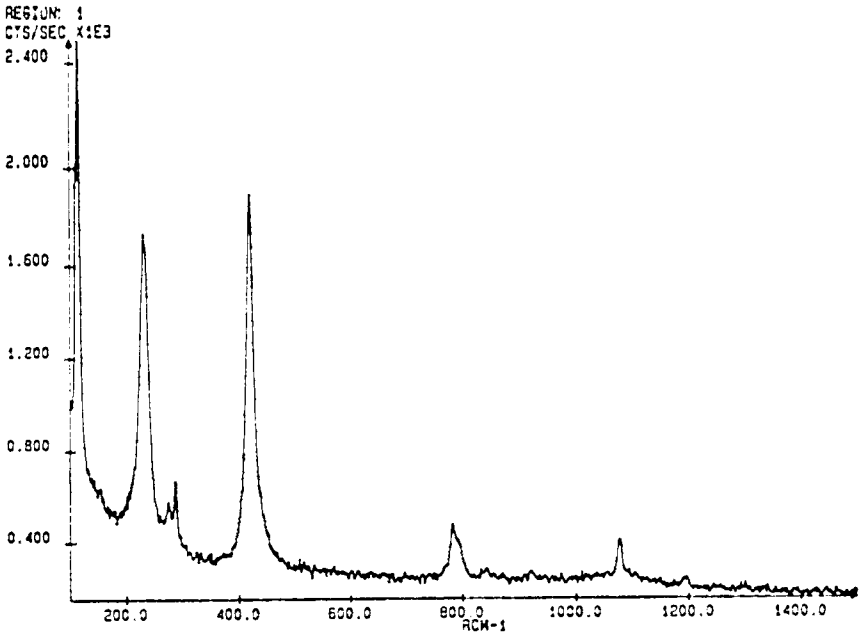

(a)

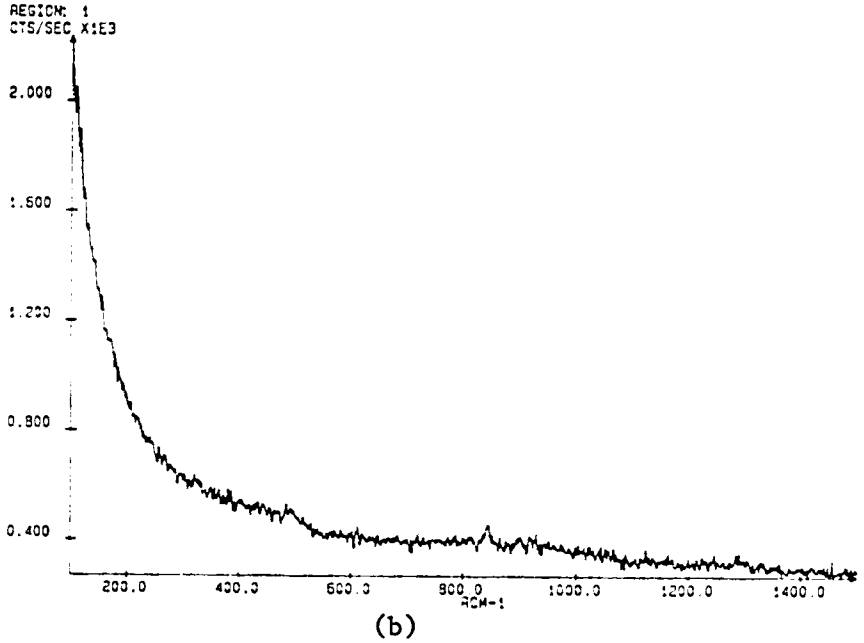

(b)

Figure 23. Raman spectrum for low cristobalite (a) and high cristobalite (b).

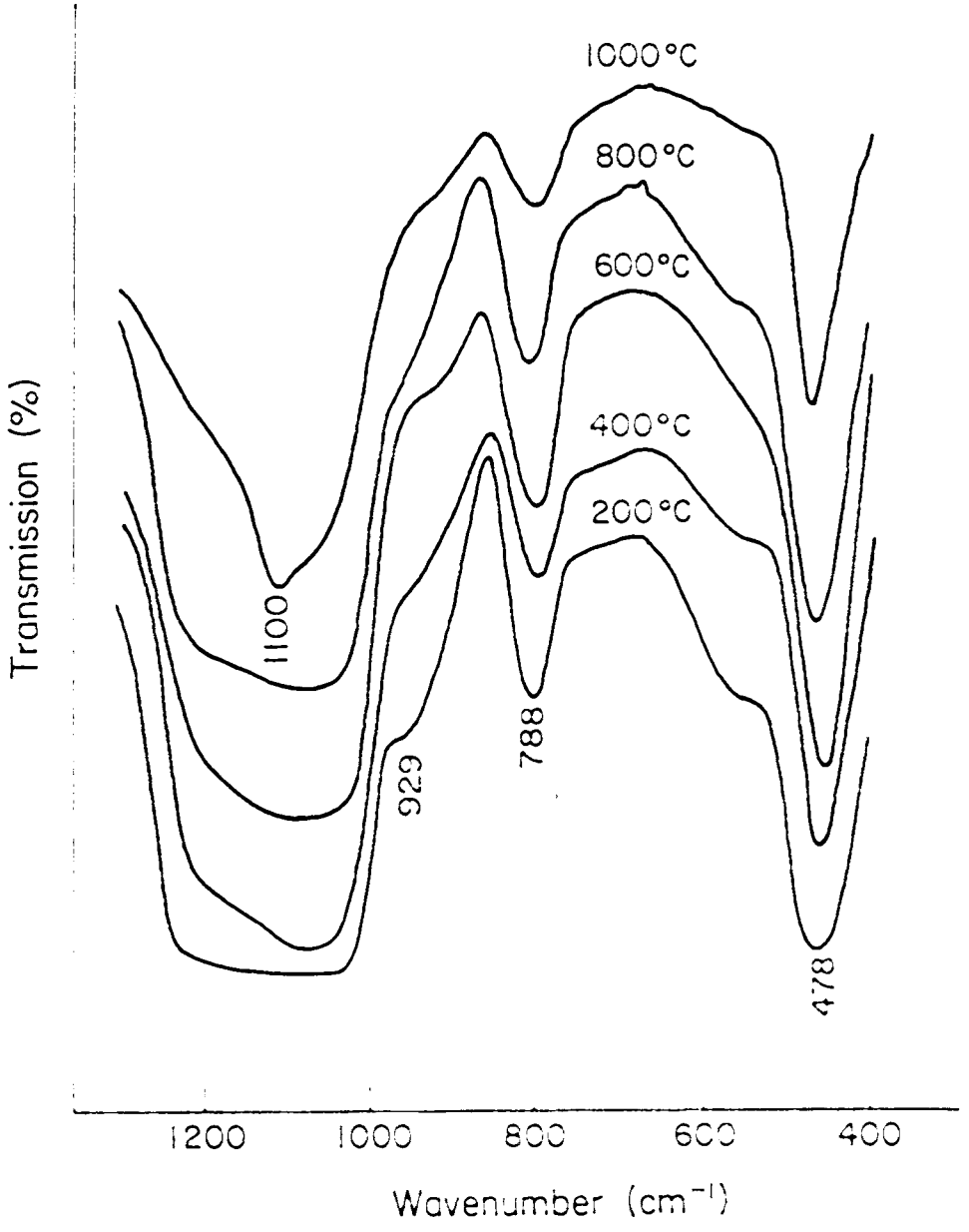

Figure 24. FTIR spectra of the gel prepared from the $CuO \cdot Al_2O_3 \cdot 30SiO_2$ composition at 200, 400, 600, 800, and 1000°C successively for 2 hours each.

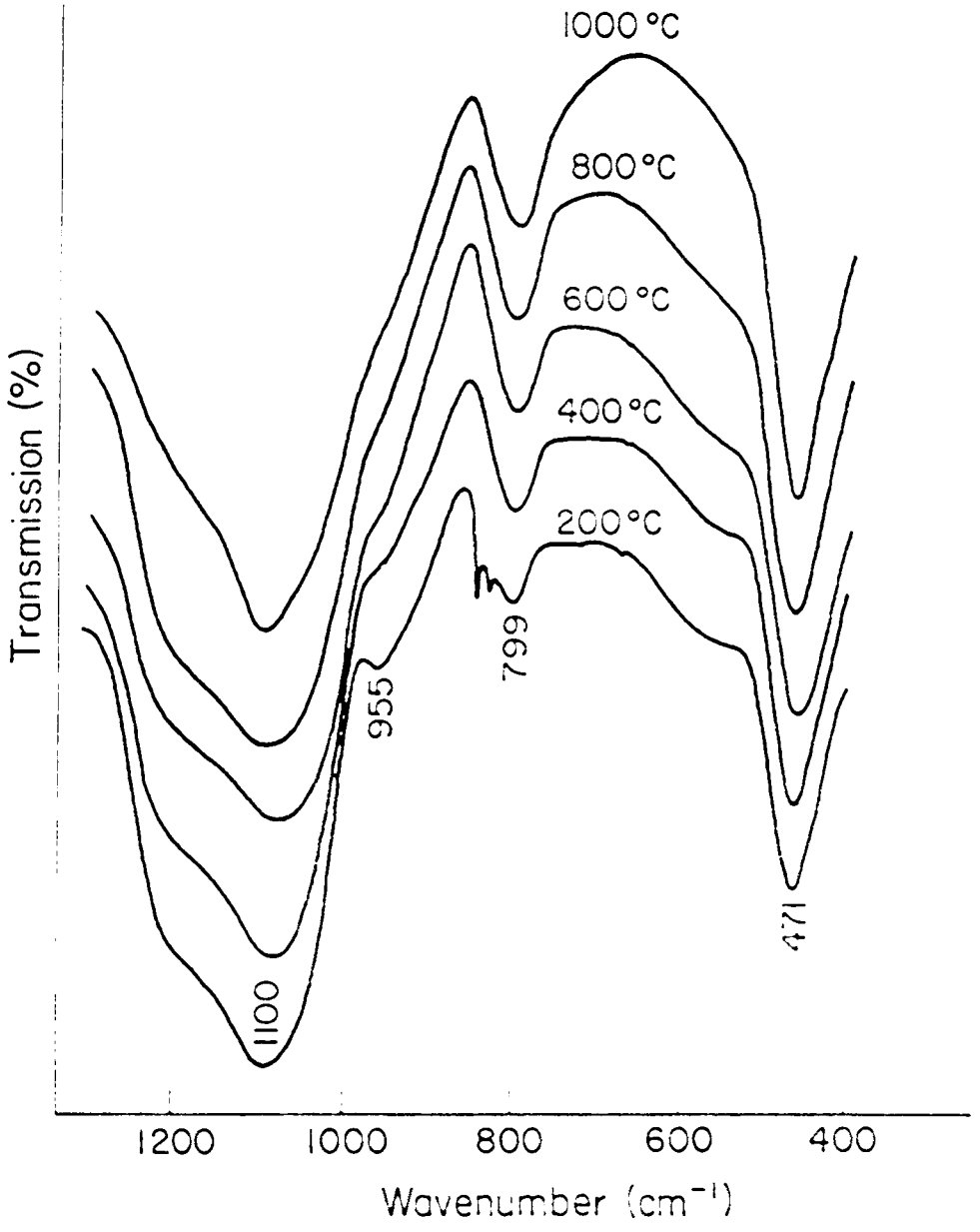

Figure 25. FTIR spectra of the gel prepared from the $CaO{\cdot}Al_2O_3{\cdot}30SiO_2$ composition at 200, 400, 600, 800, and 1000°C successively for 2 hours each.

The spikes shown in the spectrum of 200°C are probably related to artifacts.

The formation of β-quartz in the $MgO \cdot Al_2O_3 \cdot xSiO_2$ series of compositions appears to be analogous to that of β-cristobalite in the gel-to-crystal conversion. Fig. 26 shows the FTIR spectra of the xerogel prepared from the $MgO \cdot Al_2O_3 \cdot 10SiO_2$ composition. The results indicate that the β-quartz-like structure developed in the gel state subsequently crystallized into β-quartz. The spectra shown in Fig. 26, which are characteristic of β-quartz, exhibit absorption bands different from those of β-cristobalite.

The formation of β-cristobalite at a temperature far below its stability region is closely related to the local structure in its gel precursor. Despite being x-ray amorphous, the gel does seem to possess a short-range-ordered structure which resembles that of β-cristobalite. The long range order can be developed by heat treatment at 1000°C for 6 hours as evidenced by X-ray diffraction, although the heat treatment time of 24 hours was used. The fact that the gels derived from acid-catalyzed solutions fail to crystallize into β-cristobalite and the formation of β-cristobalite occurred under base-catalyzed conditions can be attributed to different gelation mechanisms. The condensation reactions in acid-catalyzed solutions take place by electrophilic attack, in which a protonated water molecule is attracted to the oxygen ions in the basic alkoxide groups.[43,44] The resulted gel consists of long linear chains with a low degree of cross-linking. On the other hand, the condensation reactions in base-catalyzed solutions proceed via nucleophilic attack,

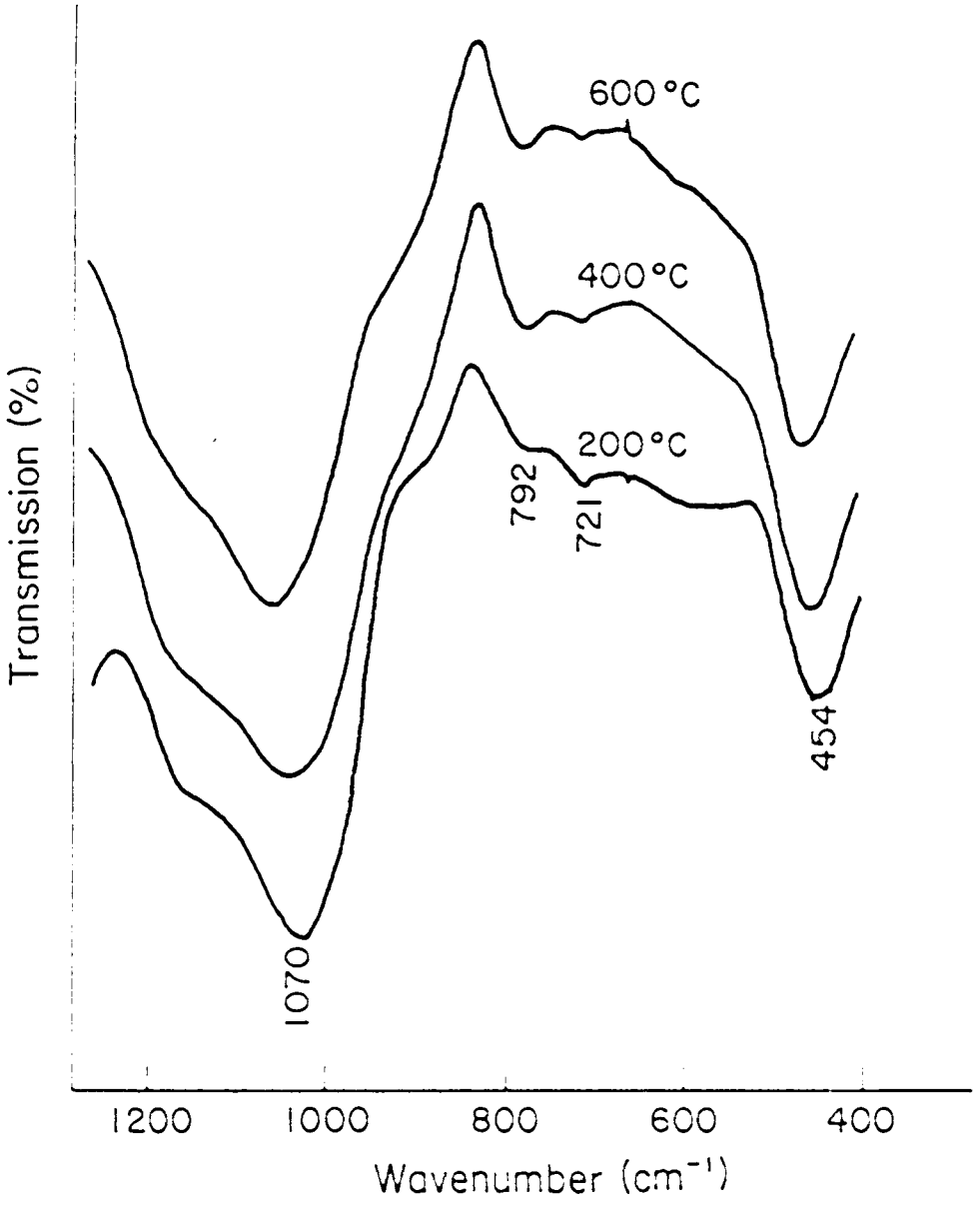

Figure 26. FTIR spectra of the gel prepared from the $MgO{\cdot}Al_2O_3{\cdot}10SiO_2$ composition at 200, 400, and 600°c successively for 2 hours each.

in which a negatively charged hydroxyl ion is attracted to a positively charged silicon, resulting in a highly cross-linked structure upon gelation. From the view point of structural similarity, the highly cross-linked polymer is much easier to convert into a framework structure than the weakly cross-linked long-chain polymer.

By the same token, the formation of β-quartz can be attributed to the same mechanism. Similar results were observed in the thermally crystallized glasses from the $(Li_2O,MgO)\cdot Al_2O_3\cdot nSiO_2$ composition.[55] β-quartz was the dominating phase even at a recrystallization temperature of 1325°C. Therefore, the crystallized phase likely inherits the local structure existing in the precursor. However, it is not clear as to what factors control the formation of the local structure. The ionic sizes of Cu^{+2} and Mg^{+2} are almost identical; however, the phases formed are completely different. It is only known that the presence of the interstitial cations and Al plays an important role in the phase formation, since neither β-cristobalite nor β-quartz can be formed for pure SiO_2 under the same processing and heat treatment conditions.

The above studies can probably shed some light on which polymorph of silica is to be used as a crystal model of silica glass. Nearly every possible form of crystalline silica had been proposed by various authors as a possible model for silica glass structure on the basis of their x-ray or infrared examinations.[56-59] Our results suggest that β-cristobalite and β-quartz are possible models for silica glass, depending on the processing conditions and on the ionic species

present in the glass.

4. Stability test

A stability test of the stabilized β-cristobalite was performed by heating the Cu series of compositions isothermally at 1250°C for 10 hours. The resulting phases and the percentages of each were determined by XRD and DSC, as shown in Table 19. The percentage of the transformed β-cristobalite was calculated by the ratio of the heat of transformation for the partially transformed β-cristobalite to that of the fully transformed phase.

The results show that almost half of the β-cristobalite phase has transformed after only 10 hours at 1250°C and no exsolution was observed. The destabilization of β-cristobalite is apparently related to grain growth at high temperature. In other words, β-cristobalite is not actually chemically stabilized, but stabilized by the grain size effect. The presence of Al and Cu^{+2} does not contribute to the stabilization, although it is crucial in forming β-cristobalite at low temperature. The effect of grain size on the stability of β-cristobalite can be made clear by including the surface energy term in the total free energy.

The total free energy of α-cristobalite and β-cristobalite can be expressed as:

$$G_\alpha = (4/3)\pi r^3 F_\alpha + 4\pi r^2 \gamma_\alpha, \qquad (1)$$

and

$$G_\beta = (4/3)\pi r^3 F_\beta + 4\pi r^2 \gamma_\beta, \qquad (2)$$

Table 19. Stability Test of the Cu-stabilized β-cristobalite Heated at 1250°C for 10 Hours.

Composition	Phase	% of conversion
$CuO \cdot Al_2O_3 \cdot 30SiO_2$	α-, β-cristobalite	44.8
$CuO \cdot Al_2O_3 \cdot 40SiO_2$	α-, β-cristobalite	48.6
$CuO \cdot Al_2O_3 \cdot 50SiO_2$	α-, β-cristobalite	48.6
$CuO \cdot Al_2O_3 \cdot 60SiO_2$	α-, β-cristobalite	49.6

assuming spherical crystals with radius r. F and γ represent the bulk chemical free energy and surface energy, respectively. For β-cristobalite to be stable at all temperatures, G_β has to be smaller than G_α, that is,

$$G_\alpha > G_\beta, \qquad G_\alpha - G_\beta = (4/3)\pi r^3(F_\alpha - F_\beta) + 4\pi r^2(\gamma_\alpha - \gamma_\beta) > 0 \qquad (3)$$

It is reasonable to assume γ_α is always greater than γ_β, since surface energy decreases with increasing temperature. Above the high-low inversion temperature T_i, $(F_\alpha - F_\beta)$ in equation (3) is always greater than zero, and therefore β-cristobalite is stable at any given crystal size. Below the inversion temperature T_i, $(F_\alpha - F_\beta)$ is negative and there exists a critical radius r_c,

$$r_c = 3(\gamma_\alpha - \gamma_\beta)/(F_\beta - F_\alpha) \qquad (4)$$

It is only when the grain size r is smaller than r_c that β-cristobalite becomes stable below the inversion temperature. When r is greater than r_c, the high-low inversion proceeds spontaneously. The $(F_\beta - F_\alpha)$ term in equation (4) becomes increasingly positive with further undercooling, indicating that r will have to be even smaller for β-cristobalite to be stable. Therefore, equation (4) basically predicts the inverse relationship between the crystal size and the transformation temperature.

In the structural investigation of opal, Buerger[2] concluded that opal is high cristobalite. Moreover, when opal was heated at about 1300°C, the x-ray pattern revealed the occurrence of grain growth and

subsequent high-low inversion of cristobalite. Studies on the tetragonal to monoclinic displacive transformation of zirconia clearly show that the tetragonal phase can be retained at room temperature when the grain size is sufficiently small.[60-63]

IV. Conclusion

The inversion temperature of cristobalite shows various degrees of dependence on solid-solution formation. Among the binary systems, lowest inversion temperature was obtained at 184°C with the addition of 10% BPO_4. The limited solubilty of TiO_2 in cristobalite accounts for the relatively high inversion temperatures in the SiO_2-TiO_2 systems. The inversion temperature of cristobalite is not strongly dependent on the presence of $AlPO_4$. For the ternary systems, the lowest inversion temperature occurred at 162°C in the SiO_2-$AlPO_4$-TiO_2 system. The inversion temperature was only moderately lowered in the SiO_2-BPO_4-TiO_2 system because of the formation of TiP_2O_7, which consumes both TiO_2 and BPO_4. Likewise, the high inversion temperatures observed in the SiO_2-$AlPO_4$-BPO_4 system are attributed to the glass formation, which presumably consumes $AlPO_4$ and BPO_4.

The stabilization of β-cristobalite appears to be controlled by the surface energy effects resulting from the formation of fine grains. By using sol-gel processing, β-cristobalite can be synthesized with small grain sizes, and more importantly at a greatly reduced temperature and time when compared to solid state reaction. Moreover, it was found that β-cristobalite is embodied in the local structure of the gel. The conversion from gel to β-cristobalite is brought about by the development of long range order at 1000°C. However, grain growth at high temperatures results in the destabilization of β-cristobalite. Changes in bond angle continue to

dominate the thermal expansion of β-cristobalite, regardless of the presence of phase transformations. Substitutions of the framework cations and the presence of interstitial cations have little effect on fixing the bond angle.

V. Reference

1. R. S. Sosman, The Phase of Silica; pp. 34-121. Rutgers University Press, New Jersey, 1965.

2. M, J, Buerger, "Crystallographic Aspects of Phase Transformation"; pp. 183-212, in Phase Transformation in Solids. Edited by R. Smoluchowski, J. E. Mayer, and W. A. Weyl, John Wiley and Sons, New York, 1951.

3. W. D. Kingery, H. K. Bowen, and D. R. Uhlmann, Introduction to Cramics; pp. 25-81. John Wiley and Sons, New York, 1976.

4. F. A. Hummel, Phase Equilibra in Ceramic System; pp. 30-38. Marcel Dekker, New York, 1984.

5. V. G. Hill, and R. Roy, "Silica Structure Studies: VI, On Tridymite," Tran. Brit. Ceram. Soc., vol. 57, 496-510 (1958).

6. W. Z. Ostwald, J. Phys. Chem., vol. 22, 289-330 (1897).

7. W. D. Kingery, Kinetics of High-Temperature precesses; pp. 222-227, Massachusetts Institute of Technology, Massachusetts, 1959.

8. S. Mitra, "Kinetics of Quartz-Cristobalite Transformation," Tran. Brit. Ceram. Soc., vol. 76, 75-73 (1977).

9. O, F, Tuttle, and J. L. England, "Preliminary Report on the System SiO_2-H_2O," Bull. Geol. Soc. Amer., vol. 66, 149-163 (1955).

10. G. R. Rigby, "Some Notes on the Mineralogy and Crystal Chemistry of Various Forms of Silica," Tran. Brit. Ceram. Soc., vol. 47, 284-291 (1948).

11. R. W. Grimshaw, A. Westerman, and A. L. Roberts, "Thermal Effects Accompanying the Inversion of Silica," Tran. Brit. Ceram. Soc., vol. 47, 269-279 (1948).

12. J. E. Stanworth," Cristobalite Inversion in a Glass Stone," Tran. Brit. Ceram. Soc., vol. 47, 280-283 (1948).

13. V. G. Hill, and R. Roy," Silica Structure Studies: V, The Variable Inversion in Cristobalite," J. Amer. Ceram. Soc., vol. 41, 532-537 (1958).

14. O. Krisement, and G. Tromel, Z. Naturf., vol. 149, 685, 912 (1959).

15. D. R. Peacor, "High-Temperature Single-Crystal Study of the Cristobalite Inversion," Z. Kristallogr. vol. 138, 274-298 (1973).

16. A. J. leadbetter, and A. F. Wright, " The α-β Transition in the Cristobalite Phases of SiO_2 and $AlPO_4$. I. X-ray Studies," Philos. Mag., vol. 33, no. 1, 105-112 (1976).

17. A. J. Leadbetter, and T. W. Smith, "The α-β Transition in the Cristobalite Phases of SiO_2 and $AlPO_4$. II. Calorimetric Studies," Philos. Mag., vol. 33, no. 1, 113-119 (1976).

18. A. Grenall, " Existence of Beta-Cristobalite at Room Temperature," J. Amer. Chem. Soc., vol. 70, no. 1, 423-424 (1948).

19. J. W. Greig, " Existence of the High-Temperature Form of Cristobalite at Room Temperature, and the Crystallinity of Opal," J. Amer. Chem. Soc., vol. 54, no. 7, 2846-49 (1932).

20. W. A. Dollase, " Reinvestigation of the Structure of Low Cristobalite, " Z. Kristallogr., vol. 121, 369-377 (1965).

21. J. J. Pluth, J. V. Smith, and J. Faber,Jr., "Crystal Structure of Low Cristobalite at 10, 293, and 473 K: Variation of Framework Geometry with Temperature, " J. Appl. Phys., vol. 57, no. 4 1045-1049 (1985).

22. M. O'Keeffe, and B. G. Hyde, "Cristobalites and Topologically-Related Structures, " Acta. Crystallogr., Sect. B, B32, no. 11, 2923-2936 (1976).

23. R. W. G. Wyckoff, "The Crystal Structure of the High Temperature Form of Cristobalite (SiO_2)," Amer. J. Sci., vol. 209, 448-459 (1925).

24 T. F. W. Barth, "The Cristobalite Structures: I. High Cristobalite," Amer. J. Sci., vol. 223, 350-356 (1932).

25. W. Nieuwenkamp, "Uber die Struktur von Hoch-Cristobalit," Z. Kristollogr., vol. 96, 454-458 (1937).

26. A. J. Leadbetter, T. W. Smith, and A. F. Wright, "Structure of High Cristobalite, " Nature (London), Phys. Sci., vol. 244, 125-126 (1973).

27. A. F. Wright, and A. L. Leadbetter, " The Structure of the β-cristobalite Phases of SiO_2 and $AlPO_4$," Philos. Mag., vol. 31, no. 6, 1391-1401 (1975).

28. J. B. Austin, " Thermal Expansion of Nonmetallic Crystals," J. Amer. Ceram. Soc., vol. 35, no. 10, 243-253 (1952).

29. L. Cartz, and J. D. Jorgensen," Pressure and Temperature Behavior of Framework Silicates and Nitrides," pp. 147-154 in Thermal Expansion 7. Edited by D. C. Larsen. Plenum Press, New York, 1982.

30. F. D. Bloss, Crystallography and Crystal Chemistry; pp. 221-282, Holt, Rinehart and Winston, 1971.

31. R. M. Hazen, and L. W. Finger, Comparative Crystal Chemistry, John Wiley and Sons, New York, 1982.

32. H. D. Megaw, "Crystal Structures and Thermal Expansion," Mat. Res. Bull., vol. 6, 1007-1018 (1971).

33. F. C. Kracek, Phase Transformations in One-Component Silicate System, pp.257-277 in Phase Transformations in Solids. Edited by R. Smoluchowski, J. E. Mayer, and W. A. Weyl, John Wiley and Sons, New York, 1951.

34. D. Taylor, "The Thermal Expansion of the Sodalite Group of Mineral," Miner. Mag., vol. 36, 761-769 (1968).

35. D. Taylor, and C. M. B. Henderson, "The Thermal Expansion of the Leucite Group of Minerals," Amer. Miner., vol. 53, 1476-89 (1968).

36. H. D. Megaw, Crystal Structures: A Working Approach, pp. 399-433, University of Cambridge, London, England, 1973.

37. H. D. Megaw, The "Thermal Expansion of Interatomic Bonds, Illustrated by Experimental Evidence from Certain Niobates," Acta. Cryst., A. vol. 24, 589-604 (1968).

38. C. M. B. Henderson, and D. Taylor, "Thermal Expansion of the Nitrides and Oxynitride of Silicon in Relation to Their Structures," Tran. Brit. Ceram. Soc., vol. 75, 49-53 (1976).

39. D. Taylor, "The Thermal Expansion Behavior of the Framework Silicates," Miner. Mag., vol. 38, 593-604 (1972).

40. D. W. J. Cruickshank, "Errors in Bond Lengths Due to Ratational Oscillations of Molecules," Acta. Cryst., vol. 9, 757-758 (1956).

41. R. K. Iler, The Chemistry of Silica, John Wiley and Sons, New York, 1979.

42. C. J. Brinker, D. E. Clark, and D. R. Ulrich, Better Ceramics Through Chemistry, North-Holland, New York, 1984.

43. C. J. Brinker, K. D. Keefer, D. W. Schaefer, and C. S. Ashley, "Sol-Gel Transition in Simple Silicates," J. Non-Cryst. Solids. vol. 48, 47-64 (1982).

44. C. J. Brinker, K. D.Keefer, D. W. Schaefer, R. A. Assink, B. D. Kay, and C. S. Ashley, "Sol-Gel Transition in Simple Silicates II," J. Non-Cryst. Solids, vol. 63, 45-59 (1984).

45. C. J. Brinker, and G. W. Scherer, "Sol-> Gel-> Glass: I. Gelation and Gel Structure," J. Non-Cryst. Solids, vol. 70, 301-322 (1985).

46. C. J. Brinker, G. W. Scherer and E. P. Roth," Sol-> Gel-> Glass: II. Physical and Structural Evolution During Constant Heating Rate Experiments," J. Non-Cryst. Solids, vol. 72, 345-368 (1985).

47. G. W. Scherer, C. J. Brinker, and E. P. Roth, "Sol-> Gel-> Glass: III. Viscous Sintering," J. Non-Cryst. Solids, vol. 72, 369-389 (1985).

48. R. W. Ricker, and F. A. Hummel, "Reactions in the System TiO_2-SiO_2; Revision of the Phase Diagram," J. Amer. Ceram. Soc., vol. 34, no. 9, 271-279 (1951).

49. E. N. Bunting, "Phase Equilibria in the Systems TiO_2, TiO_2-SiO_2 and TiO_2-Al_2O_3," J. Res. Nat. Bur. Stand., vol. 11, no. 5, 719-725 (1933).

50. R. C. DeVries, R.Roy, and E. F. Osborn, "The System TiO_2-SiO_2," Tran. Brit. Ceram. Sic., vol. 53, no. 9, 520-540 (1954).

51. W. F. Horn, and F. A. Hummel, "The System $AlPO_4$-SiO_2," Glass Ceram. Res. Bull., vol. 20, nos. 1-4, 47-59 (1979).

52. K. Okada, and J. Ossaka, "Cesium Lithium Tungstate: A Stuffed H-cristobalite structure," Acta. crystallogr., sect. B, vol. 36, 657-659 (1980).

53. W. L. Brown, R. E. Openshaw, P. E. McMillan, and C. M. B. Henderson, "A Review of the Expansion Behavior of Alkli Feldspars: Coupled Variation in Cell Parameters and Possible Phase Transitions," Amer. Mineral., vol. 69, nos.11-12, 1058-1071 (1984).

54. M. F. Hochella, JR., and G. E. Brown, JR., "Structural Mechanisms of Anomalous Thermal Expansion of Cordierite-Beryl and Other Framework silicates," J. Amer. Ceram. Soc., vol. 69, no. 1, 13-18 (1986).

55. S. Ray, and G. M. Muchow, "High-Quartz Solid Solution Phase from Thermally Crystallized Glasses of Compositions (Li_2O,MgO_2) Al_2O_3 $nSiO_2$," J Amer. Ceram. Soc., vol. 51, no. 12, 678-689 (1968).

56. J. Bock, and G. J. Su, "Interpretation of the Infrared Spectra of Fused Silica," J. Amer. Ceram. Soc., vol. 53, no. 2, 69-73 (1970).

57. E. Gorlich, K. Baszczak, and G. Sieminska, "Infra-red Studies of Vitreous Silica at Elevated Temperature," J. Mat. Sci., vol. 9, 1926-1932 (1974).

58. A. H. Narten "Diffraction Pattern and Structure of Noncrystalline BeF_2 and SiO_2 at 25°C," J. Chem. Phys., vol. 56, no. 5, 1905-1909 (1972).

59. J. B. Bates, "Raman Spctra of α and β Cristobalite," J. Chem. Phys., vol. 57, no. 9, 4042-4047 (1972).

60. R. C. Garvie, "The Occurrence of Metastable Tetragonal as a Crystallite Size Effect," J. Phys. Chem., vol. 69, no. 4, 1238-1243 (1957).

61. F. F. Lange, "Transformation Toughening, Part 1 Size Effect Associated with the Thermodynamics of Constrained Transformations," J. Mat. Sci., vol. 17, 225-234 (1982).

62. R. C. Garvie, and M. F. Goss, "Intrinsic Size Dependence of the Phase Transformation Temperature in Zirconia Microcrystals," J. Mat. Sci., vol. 21. 1253-1257 (1986).

63. R. C. Garvie, and M. V. Swain, "Thermodynamics of the Tetragonal to Monoclinic Phase Transformation in Constrained Zirconia Microcrystals," J. Mat. Sci., vol. 20, 1193-1200 (1985).

The vita has been removed from the scanned document